



Open-Channel Separation Techniques for the Characterization of Nanomaterials and Their Bioconjugates for Drug Delivery Applications

Jiwon Lee, Roxana Coreas, and Wenwan Zhong

Contents

| | | |
|-----|--|-----|
| 1 | Definition of the Topic | 114 |
| 2 | Overview | 114 |
| 3 | Introduction | 114 |
| 4 | Experimental and Instrumental Methodology | 117 |
| 4.1 | Field Flow Fractionation | 117 |
| 4.2 | Capillary Electrophoresis | 121 |
| 5 | Key Research Findings | 126 |
| 5.1 | Field Flow Fractionation for Characterization of Nanomaterials and Their Bioconjugates for Drug Delivery Applications | 126 |
| 5.2 | Capillary Electrophoresis for Characterization of Nanomaterials and Their Bioconjugates for Drug Delivery Applications | 133 |
| 6 | Conclusions and Future Perspective | 143 |
| | References | 144 |

Jiwon Lee and Roxana Coreas contributed equally to this work, with J. Lee contributing mainly to the discussion of CE related technology and development, and R. Coréas to the content about FFF.

J. Lee

Department of Chemistry, University of California-Riverside, Riverside, CA, USA

e-mail: jiwon.lee@email.ucr.edu

R. Coreas

Environmental Toxicology Graduate Program, University of California-Riverside, Riverside, CA, USA

e-mail: roxana.coreas@email.ucr.edu

W. Zhong (✉)

Department of Chemistry, University of California-Riverside, Riverside, CA, USA

Environmental Toxicology Graduate Program, University of California-Riverside, Riverside, CA, USA

e-mail: wenwan.zhong@ucr.edu

1 Definition of the Topic

Open-channel separation techniques can separate samples without reliance on column packing, minimizing sample loss due to adsorption onto the packing materials and reducing damage to samples, in particular, the complexes held together by non-chemical interactions. Field flow fractionation (FFF) and capillary electrophoresis (CE) are two representative open-channel separation techniques. In this chapter, we discuss the use of FFF and CE to separate and characterize various nanomaterials widely applied in biomedical research.

2 Overview

Nanoparticles (NPs) have facilitated advancements in disease cure and diagnosis, by enabling drug delivery, tumor imaging, and marker detection as well as other aspects of biomedical research. Thus, it is imperative to adequately access their biocompatibility and to investigate how the properties of nanomaterials, such as size, shape, charge, and composition, influence the functionality and behaviors of the nanomaterials in biosystems, which is governed by their interactions with the diverse biomolecules and biological surfaces. Many techniques have been used to characterize the biological relevant nanomaterials and study the nano-bio interface, including the open-channel separation techniques, FFF and CE. Because FFF and CE can analyze a wide range of nanomaterials composed of different chemical cores, including metals, metal oxides, semiconductors, polymers, and liposomes and exhibiting various morphology, sizes, and shapes, an assortment of separation modes and subtechniques of these two open-channel techniques have been utilized for the analysis of such materials and their bioconjugates to better assess their functionality in biosystems. Hence, in this chapter, we discuss the different approaches used in FFF and CE for such purposes.

3 Introduction

Nanomaterials have garnered appreciable significance over the years as imaging agents [1, 2], drug delivery tools [3–5], and biosensing resources [6]. Having such prodigious roles, investigating their behaviors in biological environments is of utmost importance. This is due to their potential interactions with certain biological entities such as proteins [7, 8], DNA [9], and cells [10], which greatly impacts the functionality of nanomaterials as well as raises toxicity concerns. Understanding molecular interactions and binding behaviors of nanomaterials to biological constituents have great implications in the advancement of developing nanomaterials as tools for medical research. Therefore, we begin by succinctly introducing the concepts of NP protein coronas, one example of bioconjugated NPs, and NPs for drug delivery.

Proteins and other macromolecules can adhere onto the surfaces of engineered nanomaterials (ENMs), and the resulting protein adsorption layer is termed protein corona [11–13]. In biological matrices, proteins compete to nonspecifically bind to the nanoparticle surface and lead to the formation of a protein corona [7, 14]. This corona can affect the physiochemical properties, alter the adsorption, distribution, metabolism, and excretion (ADME) profile and limit the targeting and detection capacity of NPs. Therefore, it is important to study protein corona formation on diverse nanomaterials in different biological matrices. However, the adsorption process can be quite complex in that the size, zeta potential, and surface chemistry of nanoparticles can affect the composition of the corona; in addition, the protein types and concentrations in the biological matrix also affect corona formation [7, 8]. Furthermore, there are two coronas that can adsorb onto nanoparticle surfaces: a soft corona of proteins with low binding affinity towards the nanomaterial and a hard corona with proteins that have low exchange kinetics and tend to persist longer on the nanoparticle surface. Studying the binding equilibrium of both coronas can lead to a better understanding of the toxicological mechanisms of bioconjugated nanoparticles.

The recent review by Ulbrich et al. on nanoparticles for drug delivery systems comprehensively covers the various types of NPs used, the types of drugs that have been loaded onto these particles, as well as their application in clinical trials. In this work, they address the advantages of using nanomaterials for drug delivery. Essentially, drugs that are sensitive to activation by nonspecific targets or lack water solubility can be loaded onto nanoparticles to mitigate these limitations. Additionally, nanoparticles can target specific organs or cells that the respective delivered drug cannot reach alone. For example, nanoparticles can accumulate through the leaky vasculature of tumors via an enhanced permeability and retention effect (EPR). Once these drug-loaded particles reach the targeted tumors, the drug can either be deposited or site-selectively activated and the nanoparticle itself can then be excreted [15]. The applicability of nanomaterials in medicine is extensive, thus characterization of these drug-delivery systems is indispensable.

Multiple techniques can analyze various nanomaterial characteristics. Morphology and size can be determined by microscopy techniques, such as transmission electron microscopy (TEM) and atomic force microscopy (AFM). However, sample preparation or analysis can be laborious and time-consuming. Dynamic light scattering (DLS) and nanoparticle tracking analysis (NTA) are other common techniques to evaluate the size distribution. These are nondestructive techniques, which make them ideal for analyzing nanomaterials; on the contrary, DLS may suffer in resolution [16], and both DLS and NTA have a bias towards larger particles.

On the other hand, separation techniques can be used to analyze complex biological samples, preconcentrate sample targets, and resolve sample contents, which enable them to provide a more comprehensive examination. They are also appropriate for investigating interactions since any change will be manifested in the retention time differences or shifts. Chromatography [17, 18] and gel electrophoresis [19, 20] are commonly used to separate nanomaterials. In chromatography, the efficiency of separation may be limited by the interactions of nanomaterials with

Table 3.1 Forces applied in respective field flow fractionation (FFF) subtechniques

| FFF subtechniques | Force |
|---------------------------------|---|
| <i>Flow FFF (F4)</i> | Cross flow; a second flow perpendicular to the channel flow |
| <i>Sedimentation FFF (SFFF)</i> | Centrifugal, gravitational |
| <i>Thermal FFF (Th-FFF)</i> | Thermal gradient |
| <i>Electrical FFF (El-FFF)</i> | Electrical gradient |

the column packing material and the size of the packing material. In gel electrophoresis, issues of band broadening are apparent. FFF and CE are open-channel separation techniques that can overcome these complications.

More than half a century ago, J. Calvin Giddings proposed FFF as a separation tool for large analytes [21]. FFF consists of a family of flow elution techniques, which all use open channels and applied fields to achieve differential retention of the solutes. Alteration of the force applied in FFF has resulted in multiple flexible subtechniques [22], a few of which have been listed in Table 3.1, that can separate and measure analytes simultaneously. Since its invention, FFF has been used to separate and characterize a range of samples, including but not limited to, proteins [23, 24], DNA [25], DNA-protein interactions [26], viruses [27, 28], microRNA [29], polymers [30], and more recently bioconjugated nanoparticles. FFF is an ideal tool for fractionation of complex mixtures because of its gentle interface during separations [31] and its wider analyte size range compared to other separation techniques [32]. In addition, recent developments in instrumentation and miniaturization that couple FFF with orthogonal separation or analytical techniques, like inductively coupled plasma mass spectrometry (ICP-MS), nuclear magnetic resonance spectroscopy (NMR), and multi-angle light scattering (MALS), have significantly improved the resolution of various FFF techniques and their capability in providing in-depth information of the analytes [33–35].

As pioneers, Stellan Hjertén first introduced electrophoresis in tubes in the 1970s while James W. Jorgenson and Krynne DeArman Lukacs brought capillary electrophoresis to recognition in the 1980s. Now it is a standard technique with numerous developments over the years. CE has multiple advantages over column chromatography, which include high resolution, minimal sample and reagent usage, and fast analysis; furthermore, these attributes have made CE a widely used technique in many instances for the analysis of small molecules [36], anti-cancer drugs and their metabolites [37], proteins [38], DNA [39], and enzymes [40]. In addition to the analysis of bioconjugates, drug delivery systems have been studied via CE. Various studies utilized CE to characterize the size and charge of drug delivery nanomaterials as well as assessing drug entrapment and release efficiencies.

While both open-channel separation techniques play important roles in characterization of nanomaterials employed in biomedical research and applications, including the materials employed for drug delivery, no review articles or book chapters can be found to discuss the particular contributions from both. For the ones that are dedicated to the discussion of either CE or FFF, their particular focus was on environmental, engineered, or food-related nanomaterials [41–45].

4 Experimental and Instrumental Methodology

Because our chapter involves two separation techniques, FFF and CE, they are introduced in parallel in the following sections with equal importance, i.e., discussion order is not relevant to the importance of contribution by each technique to the field.

4.1 Field Flow Fractionation

4.1.1 Flow Field Flow Fractionation

There are several advantages of applying FFF for separation of bioconjugated nanomaterials and the analysis of nanoparticles used in drug delivery. Firstly, FFF can separate analytes that range in size, from 1 nm to 100 μm , matching well with the dimensions of nanomaterials and their bioconjugates employed in biomedical research. Second, comprehensive analysis can be performed on the analyte using hyphenated instrumentation (i.e., light scattering detectors and mass spectrometers) or offline techniques after fractionation. Third, due to a lack of a stationary phase in FFF, there are no shear forces that are applied directly on the analytes. This results in a “soft” separation, which is especially ideal for proteins that may be susceptible to structural changes. Additionally, FFF channels are compatible with a range of both aqueous and organic solvents, which, in most cases, permits the analyte to retain a native state.

The most commonly used FFF technique in the analysis of nanomaterials and their bioconjugates is flow field flow fractionation (F4), because its instrumentation and implementation are simpler and relatively more mature than other FFF techniques. In addition, it is able to fractionate analytes that come in a wide size range. Thus, this part of our book chapter will focus on this particular FFF technique.

F4 instrumentation is comprised of fluid pumps, a channel, flow control units, and a sample introduction system. The basic set-up of F4 is schematically represented in Fig. 3.1. Typical F4 channel dimensions are 20–50 cm long, 2–3 cm wide, and 0.01–0.05 cm deep [46]. The channel is made by fastening a semipermeable membrane, which is permeable to the carrier but not the analyte, and a spacer between blocks that can either contain metal or ceramic semipermeable frits or are constructed of nonpermeable solid Plexiglass plate. The thickness and shape of the spacer determine the dimensions of the separation channel [24, 47]. Samples are introduced into the channel through manual injection or through an autosampler that is also typically used in high-performance liquid chromatography (HPLC).

F4 uses an axial channel flow and a perpendicular cross flow to separate analytes by hydrodynamic radii in two steps. In the first step, an external force is applied to the solute zones in the ribbon-shaped channel forcing the analytes into a narrow band on the bottom channel wall, known as the accumulation wall. This focusing step overall has no net flow of fluid along the channel and is essential to achieve good resolution. In the second step, a laminar flow, delivered by a standard HPLC pump, is applied. Common flow rates range from 0.5–5 mL/min [46]. A portion of the fluid entering the channel

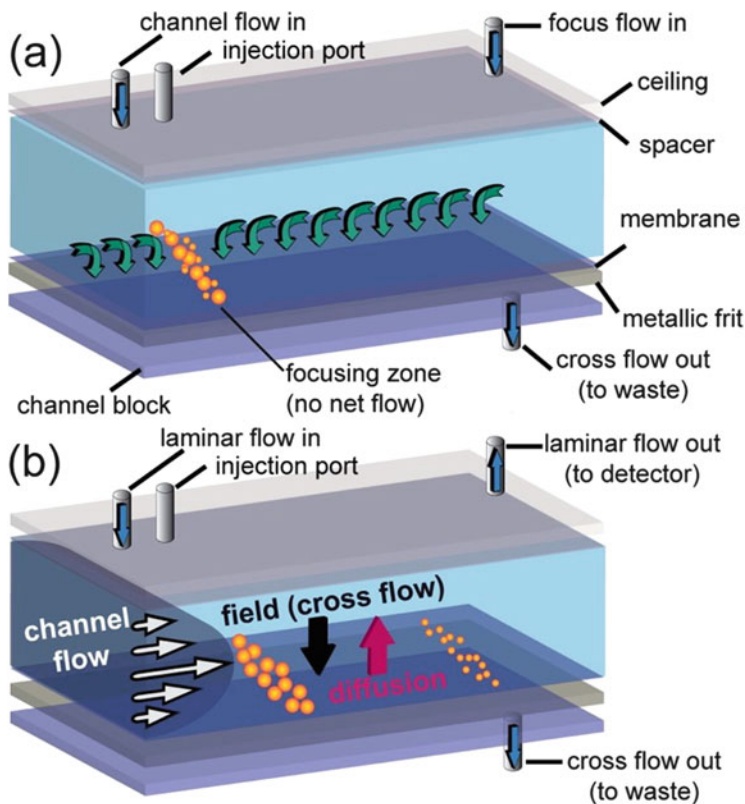


Fig. 3.1 The AF4 principle in which the eluent is pumped from the inlet to the outlet and the cross flow is applied perpendicular to the eluent flow. The first step (a) is known as the focusing step. The second step (b) is the separation process. (Reprinted with permission from Ref. [48]. Copyright 2015 American Chemical Society)

passes through the membrane to create a downward crossflow that pushes the analytes toward the membrane. The analytes then migrate back toward the channel center via Brownian motion. The remaining channel fluid flows in a laminar fashion from inlet to outlet, resulting in a parabolic elution profile. Hence, the center of this parabolic flow has a faster flow velocity whereas the edges of the channel are slower. The mass center of the analyte within this parabolic flow profile depends on the balance between its diffusion motion and the strength of the flow force: things diffusing more towards the center of the flow would be eluted earlier than those located closer to the accumulation wall. Therefore, analytes with the smallest sizes or the highest diffusion coefficients will be eluted earliest [35, 48].

Currently, there are three subtechniques of F4, which include asymmetric flow field flow fractionation (AF4), symmetric flow field flow fractionation (SF4), and hollow fiber flow field flow fractionation (HF5) [33]. Of these, AF4 is the most

developed [34]. Typical SF4 channels are symmetrical in shape, with the inlet and outlet opening in the same direction; but the most common modern instrumentation of F4 uses a trapezoidal-shaped spacer to maintain a constant axial flow velocity, and thus, is termed asymmetrical F4 (AF4) [49]. Moreover, in SF4 both of the external blocks of the channel are constructed with semipermeable porous frits, and in AF4, the bottom block contains semipermeable frits while the top block is a nonpermeable Plexiglass plate [46, 50]. HF5 is a cost-effective miniaturized FFF technique in which a hollow semipermeable polymeric or ceramic membrane serves as a cylindrical channel. HF5 can be coupled to detectors for analyte characterization.

Giddings' group explains the theory of F4 in depth [22, 23]. Briefly, the ratio between the retention time (t_r) and dead time (t_0), described by Eq. 3.1, is used to calculate the analyte retention (R) [22, 23, 50].

$$R = \frac{t_0}{t_r} \cong 6\lambda \quad (3.1)$$

The time it takes for a particle to travel through the channel without crossflow retention is referred to as the dead time and is solved by the following Eq. 3.2, in which V_0 refers to the channel void volume and V represents the flowrate of the channel [22, 50].

$$t_0 = \frac{V_0}{V} \quad (3.2)$$

The retention parameter, λ , which is related to the crossflow rate, V_c , the channel thickness, w , and the particle diffusion coefficient, D , [23] can be calculated using the following equation:

$$\lambda = \frac{DV_0}{V_c w^2} \quad (3.3)$$

At high retention levels (i.e., $R < 0.15$), t_r can be approximated with Eq. 3.4 [23]:

$$t_r = \frac{t_0 V_c w^2}{6DV_0} = \frac{t_0}{6\lambda} \quad (3.4)$$

Furthermore, using the Stokes-Einstein equation, the diffusion coefficient for spherical nanoparticles in a fluid with viscosity η , at an absolute temperature T , can be calculated by Eq. 3.5. The diffusion coefficients for proteins and other biomolecules can be acquired from literature values. The hydrodynamic radius is denoted as r_h and k_B denotes the Boltzmann's constant [32].

$$D = \frac{k_B T}{6\pi\eta r_h} \quad (3.5)$$

In order to calculate the relative recovery (RR) of nanoparticles in various carrier fluids used in FFF, Eq. 3.6 can be used, where A is the peak area of the nanoparticle in the studied carrier fluid and A^* is the peak area in the reference run.

$$RR = \frac{A}{A^*} \times 100\% \quad (3.6)$$

A deterring issue of F4 is sample loss due to analyte-membrane interactions. This can lead to inaccurate quantitation, and the collection of the fractions can be challenging. In order to minimize this loss while maximizing size resolution, extensive optimization is required of the carrier fluid composition and flow rates [51]. Therefore, for separation and characterization of bioconjugated nanoparticles with F4, carrier fluid compositions must be optimized for suitability by considering the separation of the nanoparticles as well as maintaining the integrity and native structures of the biomolecules.

Schachermeyer et al. studied the membrane adsorption of polystyrene nanoparticles and two proteins (IgG and HSA) when the carrier fluid contained various types of ionic species at high concentrations and biologically relevant pH values. Our group found that maintaining high electrostatic repulsion in F4 is essential for high recovery of NPs in high ionic strength buffers. Additionally, using weakly dissociated anions or particles conjugated with weak anions as functional groups can improve the recovery of porous nanoparticles at high ionic strengths. This phenomenon is due to the Donnan exclusion effect in which nanoparticles with higher crosslinking capacity have more occluded liquid-phase inside and are more resistant to adsorption in the carrier fluid with high ionic strength induced by weakly ionized anions [52].

With regards to the separation of proteins from nanoparticle surfaces, the protein conformation needs to be taken into consideration since the proteins ultimately determine the surface property of the nanoparticles as well as the electrostatic or hydrophobic interactions with the membrane used in FFF. Ashby et al. determined that the kinetic properties of nanoparticle-protein interactions can be probed with F4 by taking into consideration the effect of the carrier fluid on dissociation rates of proteins off of NPs, as illustrated in Fig. 3.2. Briefly, our group used F4 and LC-MS/MS to screen for proteins that bind to NPs with fast association/dissociation rates, a feature which is not possible with traditional centrifugation methods. To accomplish this feat, our group used 10 mM phosphate buffer at $\text{pH } 7.5 \pm 0.1$ with 0.025% FL-70 for the carrier fluid and 10 mM phosphate buffer at biological pH ($\text{pH } 7.4$) was used to incubate the NPs with the proteins before separation with F4 [53].

Ashby et al. used asymmetric flow field flow fractionation to separate miRNA carriers (i.e., proteins, lipoprotein particles, and exosomes) in serum and RT-qPCR to screen miRNA distributions in the carriers as a possible method to profile miRNA biomarkers for cancer diagnosis. The AF4 carrier fluid used in this study was $1 \times \text{PBS}$ (10 mM phosphate at $\text{pH } 7.4$, 137 mM NaCl, 2.7 mM KCl, and 1.0 mM MgCl_2). Extensive optimization was done on flow profiles in order to efficiently

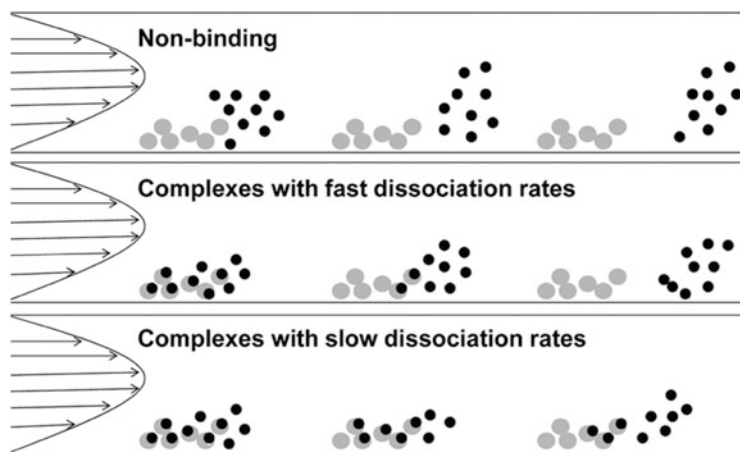


Fig. 3.2 Dissociation of proteins from nanoparticles (NPs) in AF4 allows for differentiation between the slowly and rapidly dissociating NP-protein complexes. The gray circles represent the NPs and the black circles symbolize proteins. (Reprinted with permission from Ref [53]. Copyright 2013 American Chemical Society)

separate the carriers. Ramp down of the crossflow from 3.0 mL/min to zero crossflow was analyzed over the course of 30, 20, and 15 min with the latter having better resolution and quicker elution of the analytes with little peak tailing. Also, to further improve the resolution, the crossflow was kept at 3.0 mL/min for 5 min before the 15-min ramp down, as shown in Fig. 3.3. More detail on the flow profile can be found in the article [54].

4.2 Capillary Electrophoresis

4.2.1 Capillary Zone Electrophoresis

Capillary electrophoresis (CE) consists of a bare fused silica capillary with an inner diameter typically ranging from 20 μm to 150 μm . The inlet and outlet are submerged into the background electrolyte to complete the circuit, and injection is via hydrodynamic or electrokinetic injection on the nanoliter scale. After the application of a high voltage to this system, the injected sample will be separated based on the size and charge. Each ion has its own apparent mobility, which can be calculated by the following equation:

$$\mu_{app} = \frac{L_d / t_m}{V / L_t} \quad (3.7)$$

L_d is the effective length from the inlet to the detector, L_t is the total length of the capillary, t_m is the migration time, and V is the voltage applied.

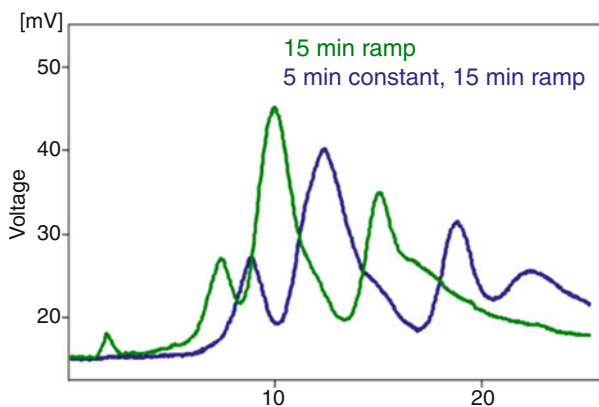


Fig. 3.3 To improve resolution of analytes, a 5-min constant crossflow was used before the AF4 separation which was performed over a 15-min ramp down from 3.0 mL/min to zero crossflow. (Reprinted with permission from Ref [54]. Copyright 2014 American Chemical Society)

The electroosmotic flow (EOF) is another component critical to CE, and it is caused by the bulk movement of the double diffuse layer, electrostatically attracted to the negatively charged silanol wall, in the background electrolyte after voltage application. The following equation explains the calculation of the EOF.

$$\mu_{eof} = \frac{\varepsilon\zeta}{4\pi\eta} = \frac{L_d / t_{\text{marker}}}{V / L_t} \quad (3.8)$$

ε is the relative permittivity of the buffer, ζ is the zeta potential of the capillary wall, and η is the viscosity of the buffer electrolyte. EOF can also be calculated using the same equation for the electrophoretic mobility, except t_{marker} is used to denote the time of an internal standard or marker. The internal standard chosen should be a neutral marker or a molecule that is only affected by the EOF. From the apparent mobility and the electroosmotic flow, each analyte's electrophoretic mobility can be obtained.

$$\mu_{em} = \mu_{app} - \mu_{eof} \quad (3.9)$$

Capillary zone electrophoresis (CZE) is the standard mode of CE. The migration order is according to the charge to size ratio in which the most positive ion with the smallest hydrodynamic diameter migrates first, and the most negative ion with the smallest hydrodynamic diameter migrates last. Figure 3.4 shows the general migration order. However, there are variations in the modes of CE as discussed in the following sections.

4.2.2 Affinity Capillary Electrophoresis

Affinity CE (ACE) is another mode of CE to study nanoparticles, and it can be applied to observe the interaction with proteins [55, 56]. Li et al. was able to

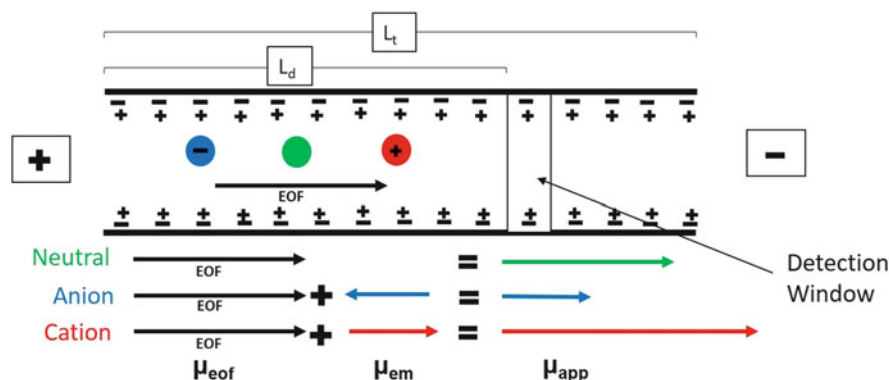


Fig. 3.4 Schematic of the separation order in CE.

differentiate between fast and slow dissociation kinetics by using both CZE and ACE to analyze the interaction between bovine serum albumin (BSA) with Fe_3O_4 nanoparticles and with Au nanoparticles [57].

Slow dissociation and fast dissociation kinetics can be analyzed using this system. For slow dissociation reactions, the nanoparticle-protein complex peak can be seen, and the peak area varies with the concentration of ligand in the background electrolyte. In this case, CZE is used. On the other hand, fast dissociation reactions can be monitored by observing the mobility shift of the receptor instead of the formation of a nanoparticle-protein complex peak. In the case of fast dissociation, ACE is used. The ratio of bound nanoparticles to total nanoparticles in CZE, θ , or the ratio of $\Delta\mu$ to $\Delta\mu_{max}$ in ACE (see Eq. 3.9), can be plotted against the ligand concentration to fit the Hill equation.

$$\theta = \frac{NP_{bound}}{NP_{total}} = \frac{(\mu - \mu_{free})}{(\mu_{max} - \mu_{free})} = \frac{\Delta\mu}{\Delta\mu_{max}} \quad (3.10)$$

μ , μ_{free} , and μ_{max} are the electrophoretic mobilities when there is a certain concentration of protein, when there is no protein, and when there is a saturated amount of protein in the background electrolyte, respectively.

Using the Hill equation, dissociation equilibrium constants and the binding cooperativity of a NP-protein complex can be calculated.

$$\theta = \frac{[protein]^n}{K_D^n + [protein]^n} \quad (3.11)$$

θ is the protein-bound nanoparticle fraction (bound nanoparticles/total nanoparticles), n is the binding cooperativity, and K_D is the dissociation equilibrium constant. The protein-bound nanoparticle fraction is based on the peak area ratio of the protein-bound and total nanoparticles. A flow chart to determine the appropriate

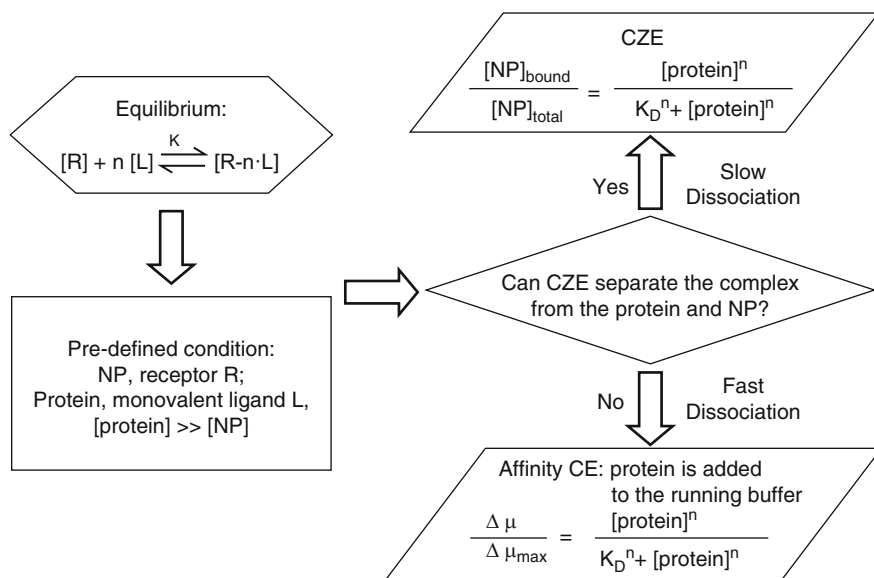


Fig. 3.5 Flowchart of CE methods for studying NP-protein interactions. (Reprinted with permission from Ref. [57]. Copyright 2010 American Chemical Society)

CE mode depending on the application is shown in Fig. 3.5 [57]. CZE and ACE can be used to understand the interactions between nanoparticles and proteins as well as extracting kinetic information.

4.2.3 Micellar Electrokinetic Chromatography

To separate neutral compounds or study an analyte with low mobility in normal polarity mode, Micellar Electrokinetic Chromatography (MEKC) is a technique commonly used for these purposes. In MEKC, surfactants are included in the background electrolyte above their critical micellar concentration. Micelles act as a pseudostationary phase, and analytes can partition between this pseudostationary phase and the aqueous phase.

Various surfactants can be used in the separation of analytes via MEKC. All surfactants have their own sizes and charges that affect their own electrophoretic mobility and their inclusion in the background electrolyte can affect the EOF. Thus, the charge and the size of the surfactant should be considered when designing MEKC methods. The most commonly used surfactant is sodium dodecyl sulfate (SDS), which was also notably used in the first development of MEKC [58]. SDS carries a negative charge to create a delay in the migration time of the analyte. Other common surfactants include positive ones, such as cetrimonium bromide (CTAB) and tetradecyltrimethylammonium bromide (TTAB), as well as nonionic ones, such as Brij-35 and Tween 20. Depending on the purpose, the most suitable surfactant can be chosen for separation in CE. For application to nanomaterial separations, SDS has been the prevalent option.

The use of SDS can improve the separation of metal nanoparticles. Liu et al. found that 5.3 and 19 nm AuNPs could not be separated with good resolution when the background electrolyte did not include SDS. SDS can adhere to the surface of AuNPs, affecting their surface chemistry, and act as their stabilizers as well. Due to the adsorption of SDS molecules, the concentration of the surfactant can affect the electrophoretic mobility of AuNPs; furthermore, the trend of change in electrophoretic mobility depended on the size of the nanoparticles. At lower surfactant concentrations, the charge-to-size ratio of small nanoparticles is larger. On the contrary, the charge-to-size ratio of larger nanoparticles is larger at higher surfactant concentrations. This is due to the charge of the nanoparticle not being limited by the number of SDS molecules allowed to attach to the surface at higher concentrations of SDS, and larger nanoparticles have more surface area to link to SDS molecules [59].

Ciriello et al. used a stabilizer, poly(sodium4-styrenesulfonate) (PSS), for the separation of AuNPs with sizes ranging from 5 to 20 nm. Similar to the behavior of SDS, PSS can adhere to the surface of AuNPs and induce an electrophoretic mobility difference and a modification of the EOF. This polyelectrolyte contains a hydrophobic and negatively charged hydrophilic portion, providing an electrostatic and steric stabilization and prevention of aggregation when adsorbed onto AuNPs. They found a saturation percentage of 1% PSS in which AuNPs are fully covered by the PSS molecules. They validated their technique by comparing with the sizes of nanoparticles found in transmission emission microscopy. In addition, the addition of PSS creates an electrophoretic drag that can improve separation of AuNPs [60]. In general, several parameters, such as buffer concentration, buffer pH, buffer type, voltage, and injection type (hydrodynamic vs. electrokinetic), need to be considered for CE analysis as these can affect separation.

4.2.4 Separation Efficiency

Assessment of CE performance and separation efficiency is important, and the sharpness and distance between peaks need to be optimized. They can be evaluated based on the resolution of peaks and the theoretical plate number. Plate height number is used in the evaluation of other chromatographic techniques as well, and it is defined by the relationship where L = length of the column and N = theoretical plate number.

$$H = L/N \quad (3.12)$$

The number of theoretical plates is defined as the following:

$$N = \frac{L_d^2}{2Dt_m} = \frac{(\mu_{em} + \mu_{eof})VL_d}{2DL_t} \quad (3.13)$$

where L_d is the effective length from the inlet to the detection window, D is the diffusion coefficient of the solute, t_m is the migration time, μ_{em} is the electrophoretic mobility, μ_{eof} is the electroosmotic flow, V is the voltage applied, and L_t is the total length of the capillary.

Peak resolution is defined by the ratio of the difference in migration times and the average of the width of the two peaks.

$$R = \frac{t_A - t_B}{W_{b,avg}} \quad (3.14)$$

t_A = migration time of peak A , t_B = migration time of peak B , and $w_{b,avg}$ is the average peak width of the two peaks at baseline. By calculating these variables, the separation performance in CE can be evaluated and validated.

5 Key Research Findings

Apart from the electrical, optical, and magnetic properties that nanomaterials individually possess, which allot their use as effective biomedical tools, conjugation with proteins, oligonucleotides, drugs, and other biomolecules is a critical step that facilitate their applications in biomolecular assays, in vivo imaging, and cancer targeting therapeutics [61, 62]. In the following sections, we will review analytical studies on the separation and characterization of bioconjugated as well as drug-loaded nanomaterials via FFF and CE.

5.1 Field Flow Fractionation for Characterization of Nanomaterials and Their Bioconjugates for Drug Delivery Applications

Many of the applications of SF4 or AF4 have been centered on characterizing nanomaterials prepared for biomedical purposes, such as drug delivering nanoparticles and nano-sized materials for target imaging. These nanoparticles are mainly metal oxide, metal, quantum dots, liposomes, and the bioconjugated entities. The works reviewed below will prove the utility of this technique in analysis of nanomaterials and their bioconjugates including medicinal molecules.

5.1.1 Metallic Nanoparticles

Metallic nanoparticles are becoming more frequent in medical applications and in sensors because of their reactive surfaces and unique optical properties. For example, gold nanoparticles (AuNPs) have been used optimized as nanozymes for aptasensor applications [63] and silver nanoparticles (AgNPs) have been complexed as highly selective fluorescent nanosensors for dopamine [64]. Herein we present articles that have applied FFF for the characterization of metal-based nanomaterials conjugated with biomolecules.

Safenkova et al. conjugated eight distinct antibodies from immunoglobulin G (IgG) to AuNPs, which were separated with AF4 and characterized by MALS, UV-Vis, and DLS. These bioconjugated AuNPs were prepared in three different ways: with a single conjugate, in a mixture of all eight antibodies, and in a

concentrated solution of all eight antibodies. They found that the mixtures of the eight conjugates had equal average radii compared to the single conjugated sample and that the concentration of the conjugate did not influence the size. In addition, they found that the AuNPs alone had a different distribution compared to the bioconjugated materials. Essentially, the AuNPs alone were monomodally distributed and the bioconjugated AuNPs were bimodally distributed with the second population of the latter being a structural influence from the conjugate during synthesis [65].

Although AgNPs have been separated by AF4 extensively [66, 67], their separation with hollow fiber F4 (HF5) has only recently been studied. HF5 was coupled to MALS for the characterization of AgNPs coated with either polyvinylpyrrolidone (PVP) or PVP with SiO₂. PVP is a water-soluble polymer used as a binder in the production of medical drugs. Regardless of coating, the fractograms displayed no void peak and showed that these types of coatings did not influence the elution time of the AgNP peak. Surprisingly, dilution of the coated AgNPs changed the overall shape of the particle from rod- and chain-like to spherical morphologies due to agglomeration events which were measured through the release of Ag⁺ ions [68]. The authors have also separated solid AgNPs from dissolved Ag⁺ ions with HF5 [69].

AF4, hyphenated to UV-Vis and ICP-MS, has also been used to determine the protein corona formed on AgNPs after incubation with plasma proteins. Wimuktiwan et al. found that within 5 min of incubation, a stable protein corona was formed, shown in Fig. 3.6. Additionally, after 24 h, they were able to identify the protein-corona stabilized AgNPs with AF4. However, the group did not assess the corona formation after incubation with protein-rich plasma itself [70].

Selenium nanoparticles (SeNPs), which can catalyze the generation of superoxide anions, have been applied in nanomedicine as drug carriers [71] and potential chemotherapeutic agents [72]. Their use as delivery agents has been supported due to the fact that these materials do not induce toxicity at low doses. Although most characterization of SeNPs occurs during synthesis, this method does not account for the alteration stabilizers, biomolecules, or biological matrices have on the sizes of SeNPs.

Pornwilard et al. studied the effect of gastrointestinal conditions (shifting the pH of the solutions to pH 2 for gastric and to pH 7 for intestinal conditions) on SeNPs through characterization with AF4-ICP-MS. They used biomolecules (pectin, alginate/pectin, ovalbumin, and β -lactoglobulin) to coat SeNPs before incubation in the two solutions that mimic gastrointestinal fluids. They found that there were shifts in the fractograms of SeNPs after incubation in the GI conditions, due to the chemistry of the conjugates. At pH 2, all four coating molecules were negatively charged, while at pH 7 only the two proteins were negatively charged. They found that the GI conditions, as well as the bioconjugates, stabilized the SeNPs. Additionally, they looked at the effects of adding enzymes into the two GI-conditioned SeNPs. For the polysaccharide coated particles at pH 2, there was a decrease in size after the introduction of pepsin (an enzyme to mimic the GI conditions of the stomach) to the pectin coated particles but no size change in the alginate/pectin conjugated

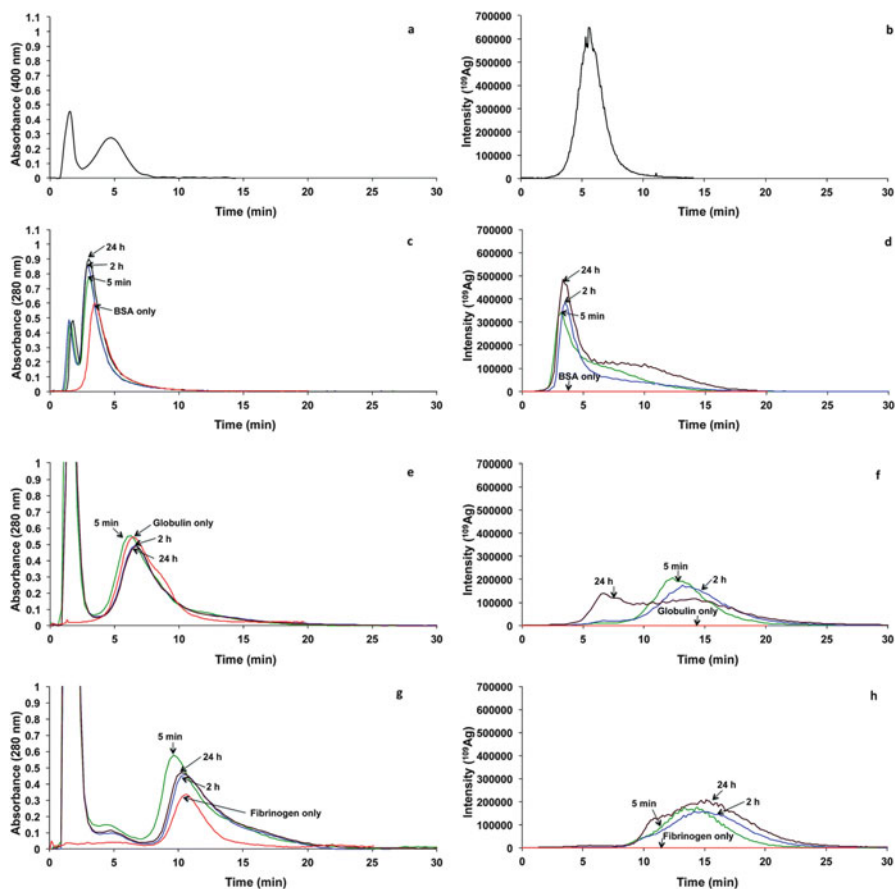


Fig. 3.6 Fractograms of 2.6 nm tannic stabilized AgNPs with UV-Vis (a, c, e, g) and ICP-MS detection (b, d, f, h). The AgNPs were incubated with BSA (c and d, red), globulin (e and f, red), and fibrinogen (g and h, red) for 5 min (green), 120 min (blue), and 24 h (brown). (Reproduced from Ref. [70]. Copyright 2015 The Royal Society of Chemistry)

particles. For the protein coated materials, incubation with pepsin resulted in a size increase for ovalbumin coated particles and the loss of the second peak seen in β -lactoglobulin coated SeNPs. At pH 7, they used pancreatin-bile extract as the enzyme to mimic the GI conditions of the intestine. They observed a decrease in size for all materials regardless of coating due to an increase in electrostatic repulsions. Regardless of the shifts they observed, more than 90% of SeNPs were present after the GI digestion and fractionation with AF4 [73].

5.1.2 Metal Oxide Nanoparticles

Metal oxide nanoparticles are extensively used in industry, agricultural products, medicine, and cosmetics [74]. For example, superparamagnetic iron oxide

nanoparticles (SPION) have been modified for chemotherapeutic applications [75]. Zinc oxide (ZnO) and titanium dioxide (TiO₂), which can be dispersed in a variety of materials, from personal care products to sensors, possess antimicrobial and disinfecting properties. Therefore, these materials have been increasingly used in nanomedicine as drug carriers with antibacterial capacities [76, 77]. The following articles used FFF for the separation of bioconjugated metal oxide nanoparticles.

Our group studied the formation of the protein corona on SPIONs after incubation in depleted human serum with AF4 by screening SPION-protein interactions based on dissociation rates [53], and we isolated the SPIONs with the intact hard corona [78]. The size of the SPIONs clearly increased after incubation with the serum, as inspected by AF4. The proteins in the hard corona were digested and analyzed with 2-dimensional nano-LC-MS/MS to determine the protein composition of both the soft and hard coronas, which is schematically represented in Fig. 3.7. We found that increasing the NP core size as well as using hydrophobic surface ligands attracted more proteins to form a more dynamic corona. These studies demonstrate the utility of an open-channel separation technique like AF4 in elucidating the formation of the protein corona, which can be useful in guiding the design of biocompatible nanomaterials for medical applications.

5.1.3 Polymeric Nanoparticles

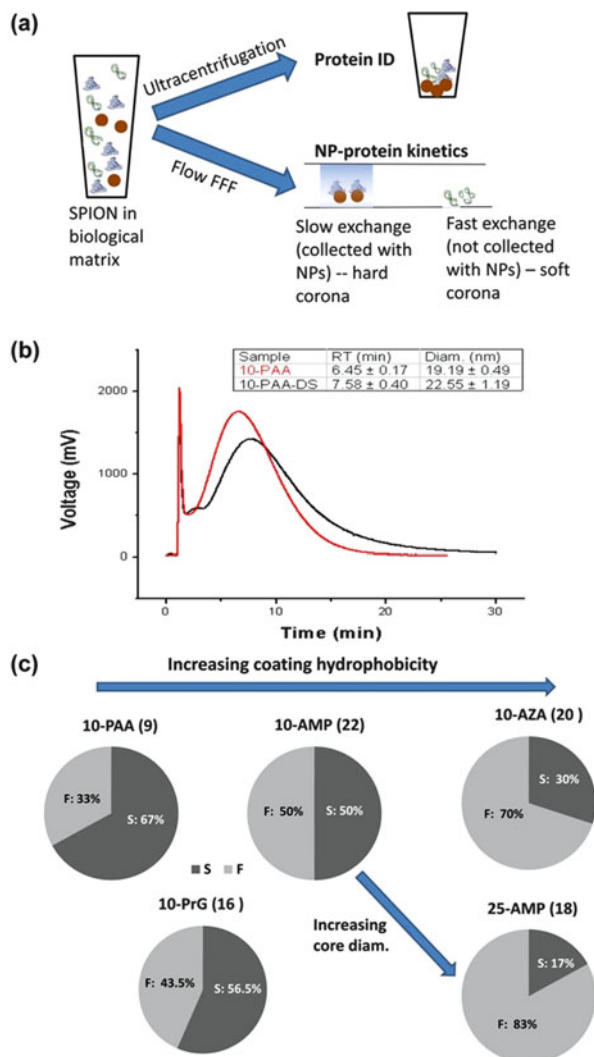
Polystyrene nanoparticles are versatile materials due to their stability in simple dispersants and complex matrices as well as their low toxicity and ability to be effortlessly functionalized. Here we introduce studies that have applied FFF for characterization of bioconjugated nanomaterials as well as drug-loaded particles for drug delivery.

Weber et al. used AF4 to separate free plasma proteins, without disturbing the weak interactions of low affinity proteins, from the surfaces of polystyrene nanoparticles. After incubation in serum, this group used centrifugation to separate the hard corona proteins and used AF4 for the soft corona which contains the low affinity proteins. This conclusion contradicts with what we have found in our work [53, 78] probably due to differences in the flow conditions, channel thickness, and membrane pore size used in these two studies. The authors confirmed the corona compositions with SDS-PAGE and LC-MS and found that the principal component that adsorbed onto the particles was the low-binding affinity protein, human serum albumin [79].

An evolving category of nanoparticles are metal organic framework (MOF) materials which exhibit very large surface areas. These particles are 3D porous inorganic polymer clusters or crystals composed of metal ions and are assembled together with organic ligands. Due to their ability to be modified readily, MOFs can be used in multiple applications ranging from sensors to drug delivery [80].

Recently, Roda et al. loaded MOFs with nucleoside reverse transcriptase inhibitors (NRTIs) for drug delivery in HIV therapy. The direct administration of NRTIs is complicated; poor stability of these types of drugs in biological media limits cellular uptake while the inefficiency of intracellular kinases to metabolize the drugs into the correct derivatives reduces the drugs ability to act as a therapeutic. Not only do

Fig. 3.7 (a) The scheme for determination of the hard and soft corona formed around SPIONs. (b) Fractograms of SPIONs functionalized with the surface ligand 10-PAA (red) and 10-PAA incubated with depleted serum (black). (c) The pie charts quantify the percentage of proteins identified in the hard (dark gray) and soft (light gray) corona. S stands for slow exchange and F for fast exchange. The number in parentheses, following the name of the nanomaterial, represents the total number of proteins identified in the corona. (Reprinted with permission from Ref. [78]. Copyright 2014 ACS Applied Materials & Interfaces)



MOFs overcome these two issues, due to their ability to stabilize the drugs and their derivatives, but also their nontoxic nature makes them optimal drug delivering nanoparticles [81]. Roda et al. examined empty MOFs and correlated the size changes after loading the MOFs with azidothymidine (AZT, a commonly used NRTI drug) azidothymidine monophosphate (AZT-MP) and azidothymidine triphosphate (AZT-TP) with the AF4-MALS results. They measured the particle size distribution (PSD), obtained with the AF4-MALS root mean square (rms) radius values. Both the empty MOF and the MOF-AZT samples had identical PSD values at approximately 81 nm while the MOF-AZT-MP and MOF-AZT-TP had radii of 90 and 97 nm, respectively. These size increases for the phosphorylated drug

MOF-delivering samples were attributed to the binding and bridging effects of the drug to the MOFs. Interestingly, this group found that, although the theory of FFF suggests that smaller particles elute first, the smaller unloaded MOFs eluted slower than the larger drug-loaded MOFs. They found that the zeta potential of their samples played a critical role in this elution order due to the two phosphorylated drug-loaded MOFs having negative zeta potentials; therefore, these particles would be repelled away readily from the negatively charged polyethersulfone membrane channel compared to the empty MOF which is smaller in size but has a positive zeta potential. Additionally, this group studied the morphological stability of the loaded MOFs after 24 h. Ultimately, each of the loaded MOFs as well as the empty MOF were stable over time. The tri-phosphorylated drug was more stable in the MOF, compared to the monophosphorylated drug, and this could be due to the binding constant of the drug to the MOF being higher for the tri-phosphorylated drug [81].

5.1.4 Liposomes

Liposomes are biocompatible drug delivering carriers due to their hydrophobic interactions with cellular receptors. The subsequent articles focus on the analysis of bioconjugated NPs and drug delivery NPs through the application of FFF.

Hinna et al. used AF4 to measure the exchange between small-drug-loaded liposomes with large acceptor liposomes that mimic the interactions between the carrier liposomes and “biological sinks.” The drug they used was p-THPP (5,10,15,20-tetrakis(4-hydroxyphenyl)21H,23H-porphine). After preparing the liposomes, they used AF4 to determine the size distribution of both donor and acceptor liposomes and they were able to reproducibly separate these two species, depicted in Fig. 3.8. They then coupled AF4 with UV-Vis and off-line HPLC to quantify the model drug content in the donor and acceptor fraction; they simultaneously quantified drug transfer and release to an aqueous phase and determined the transfer kinetics of p-THPP to be first order with a half-life of 300 min [82].

Targeted alpha (α)-particle therapy (TAT) is a form of radioimmunotherapy in which nuclides decay into radioactive daughters emitting α -particles that kill tumor cells, via short 70–100 μm energy paths, while evading surrounding normal cells [83]. TAT is considered to be both highly potent and specific in the therapeutic application for ovarian, breast, colon, and prostate cancers. Nanomaterials have recently been considered as vectors capable of transporting α -emitting particles to cancer cells. However, a limitation in using these vectors is keeping the daughter isotope bound to the nanomaterial after the parent nucleoside decays and emits the α -particle.

Huclier-Markai et al. monitored the stability of lead-212 (parent nuclide)/bismuth-212(daughter isotope) radionuclide pair encapsulated by liposomes in vitro using AF4 coupled to MALS and a gamma (γ) ray detector. This group began their analysis by preparing liposomes with an average diameter of 109 nm and a polydispersity index of 0.119, optimal for use in TAT. They then labeled the liposomes in two different manners. One set of the liposomes were labeled with indium and the other set was labeled with indium and also encapsulated ^{212}Pb . Using AF4 with a cellulose membrane, coupled to MALS and a UV-VIS detector, they found that there

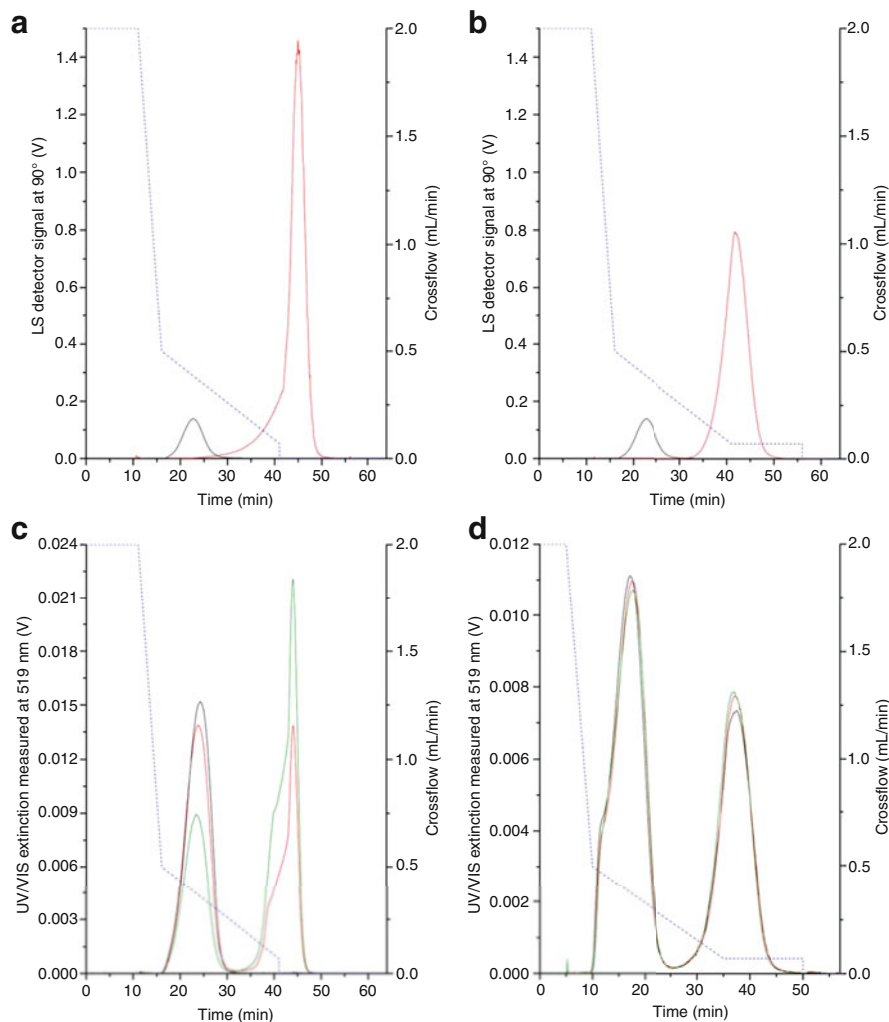


Fig. 3.8 (a and b) Fractograms of (black) donor liposomes were overlaid with those of (red) acceptor liposomes. The dashed blue lines represent the applied crossflow gradients. (a) Donor and acceptor liposomes were prepared by slow extrusion through polycarbonate membranes and were fractionated using a method where zero crossflow was attained around 41–42 min. (b) Donor and acceptor liposomes were prepared by extrusion, freeze-thaw, centrifugation, and fractionated over non-zero crossflow. (c) Fractograms of overlaid (black) donor liposomes with transfer experiment aliquots at (red) 0 min and (green) at equilibrium. (d) Overlaid fractograms of liposomes incubated within channel under low focus flow for (black) 10, (red) 30, and (green) 60 min. (Reprinted with permission from Ref. [82] Copyright 2016 Journal of Pharmaceutical and Biomedical Analysis)

was no significant size increase between the unlabeled liposomes, the indium-labeled liposomes, and the ^{212}Pb encapsulating liposomes and the three different liposome samples eluted at approximately 11 min. Additionally, through the use of the γ -ray detector, the group observed a signal at the 11 min retention time for the

^{212}Pb encapsulating liposomes and calculated 86% efficiency in radiolabeling the liposomes. They measured the stability of ^{212}Pb in liposomes after these species were incubated in human serum for 20 h and found that more than 85% of the liposomes encapsulating ^{212}Pb were stable in the matrix and did not release the daughter isotope. These results are notable due to the fact that the liposomes have a biological period of 14 h in mice and therefore there is both sufficient time for the ^{212}Pb encapsulating liposomes to reach cancerous cells, decay (the half-life of ^{212}Pb is 10.6 h), and release α -particles that can kill cancer cells [84].

5.1.5 Quantum Dots

Quantum dots (QDs) are luminescent semiconductor nanoparticles. Due to their optical properties, QDs are used in multiple applications including sensors and drug delivery. In biological applications, QDs are conjugated with a specific antibody or aptamer for therapeutic and in-vivo applications in complex matrices. The studies mentioned below use FFF for the separation and analysis of bioconjugated QDs.

Moquin et al. investigated the effects of cell culture media on the stability of QDs as well as the time-dependent effects on the hydrodynamic diameters using AF4 coupled to MALS, DLS, and UV-Vis detectors. They coated the CdSe (CdZnS) nanomaterials with three negatively charged ligands and then incubated the QDs in cell culture media. They found that after 24 h, the sizes of the QDs incubated in cell culture media were larger than those of QDs dispersed in water when the QDs were capped with mercaptopropionic acid (MPA) or dihydrolipoic acid (DHLA). The latter had the most dramatic size increase indicating hefty agglomeration, illustrated in Fig. 3.9. This was slightly observed in QDs coated with α -carboxyl- ω -mercapto poly(ethylene glycol) (PEG-COOH) denoting that this ligand was influential in the QDs stability in cell culture media [85].

Bouzas-Ramos et al. coupled AF4 to an ICP-MS to investigate the purification of one-pot synthesized QDs. These materials were separated with AF4 after being capped with ligands that can functionalize to antibodies [86]. This technique can be used to assess the integrity of these materials before their applications in biomedicine.

Menéndez-Miranda et al. used AF4 with on-line ICP-MS to measure conjugation effectiveness between monoclonal IgG antibody and CdSe/ZnS core shell QDs. In order to calculate the bioconjugation efficiency, they used four different molar ratios for analysis with AF4. They found that increasing the QD: antibody ratio would result in an increase in bioconjugation with a 75% efficiency using a 3:1 ratio [87].

5.2 Capillary Electrophoresis for Characterization of Nanomaterials and Their Bioconjugates for Drug Delivery Applications

CE is also quite comprehensive in its analysis of nanomaterials, and separation can be enhanced by selecting the optimal CE mode as described in the experimental section. CE can be applied to the separation of metallic nanoparticles, metal oxide

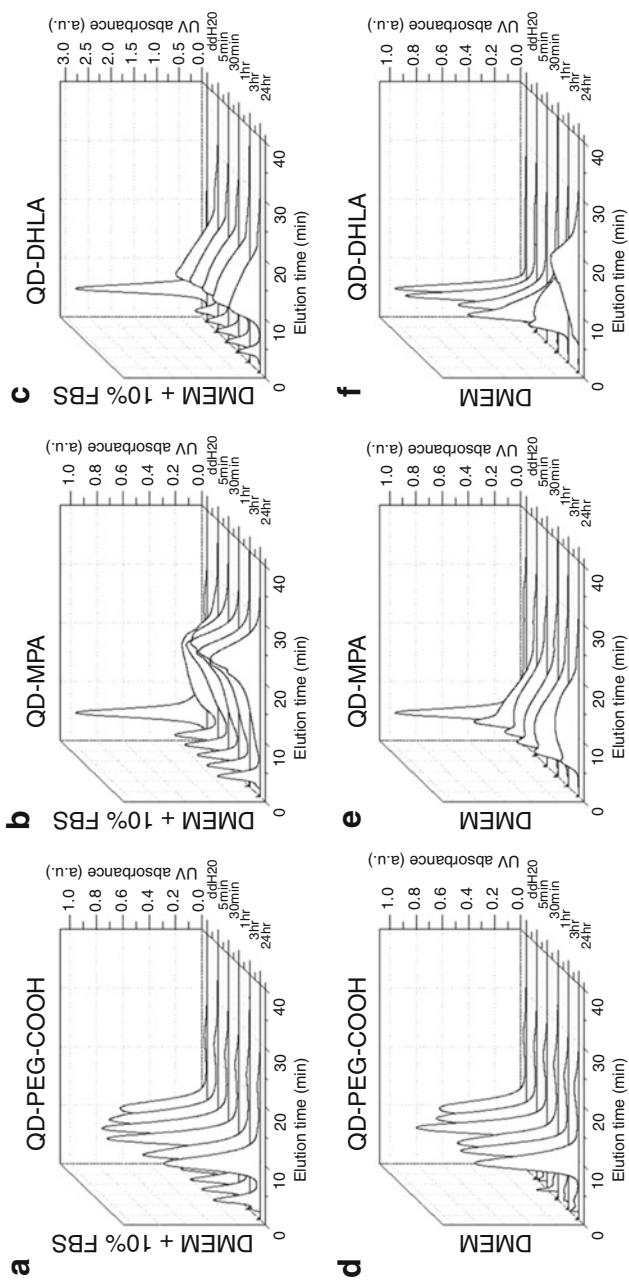


Fig. 3.9 Fractograms of the agglomeration phenomenon of QDs suspended in DMEM (bottom) and DMEM with 10% FBS (top) over 5 min, 30 min, 60 min, 3 h, and 24 h. (Reprinted with permission from Ref. [85]. Copyright 2015 European Journal of Pharmaceutics and Biopharmaceutics)

nanoparticles, polymeric nanoparticles, and quantum dots for the use as imaging tools, delivery agents, and biosensor components. In the following section, we will discuss the most recent revelations for various nanomaterial types.

5.2.1 Metallic Nanoparticles

Many recent key findings for metallic nanoparticles have focused on protein binding. When administering drug delivery nanomaterials into biological systems, it is imperative to understand nanoparticle-protein interactions and how they affect the process of targeting to specific sites. Matczuk et al. studied AuNPs and their interaction with proteins using CE coupled to ICP-MS. The authors first optimized the conditions for CE in order to analyze their samples. They found the best buffer to be 40 mM HEPES at a pH of 7.4 to ensure physiological conditions as well as optimal separation. 15 kV separation voltage and a sample loading pressure of 20 mbar for 5 s were chosen to reduce peak broadening and analysis time as well as prevent protein adsorption to the wall from sample overloading, which shows that optimization of the conditions is highly imperative to CE separation. The method was validated and found to be reproducible by comparing the migration time of AuNPs to that of AuNP-albumin conjugates and comparing the peak areas for intraday and interday analysis. After they calculated capillary recovery values, they found that there was a decrease in the capillary recovery with their largest AuNP at 50 nm due to adsorption of larger proteinaceous conjugates to the capillary wall [88], which can be avoided by a dynamic or permanent coating of the wall [89].

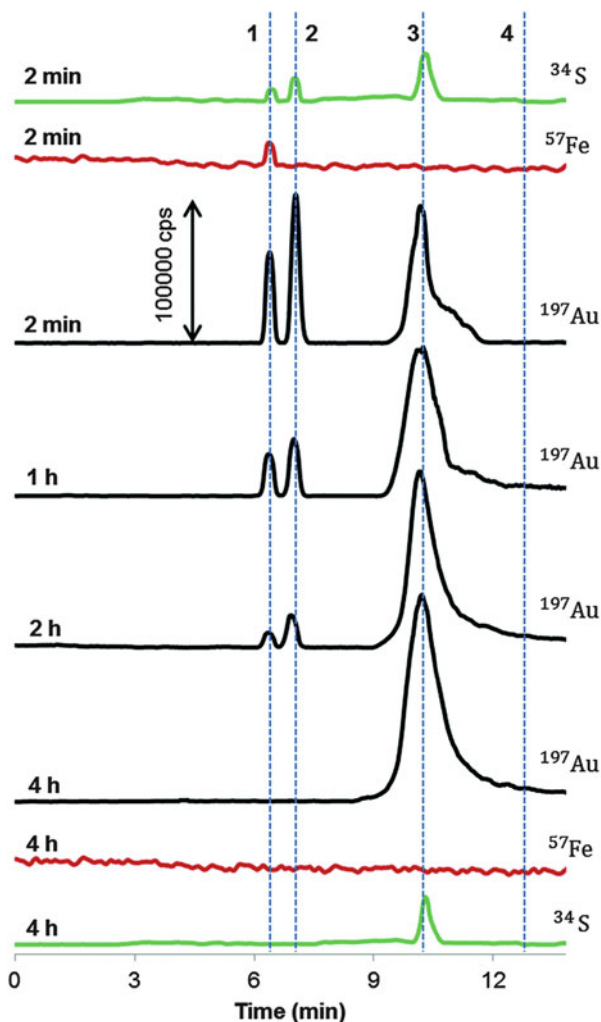
After optimization, Matczuk et al. explored the interactions between individual proteins and AuNPs. First, they found that the interaction between albumin and AuNPs is fast for 10-, 20-, and 50 nm sized particles in that binding was complete after 5 min. However, with 5 nm particles, the interaction is fast in the first 5 min but decelerates afterwards. They explained this mechanism as the change in albumin's structure after binding to nanoparticles over time [88].

Matczuk et al. then observed the interaction of AuNPs with two forms of transferrin: holo-transferrin and apo-transferrin. Again, the kinetics were fast in that equilibrium was attained after 5 min; however, there were more unbound nanoparticles at equilibrium. The authors then proceeded to study the interaction between different proteins in human serum to mimic a real biological system. As seen in Fig. 3.10, they found that albumin was the only protein participating in corona formation, and it eventually displaced the two forms of transferrin due to the contents in the serum matrix [88]. The paper emphasizes the interesting phenomenon of protein-NP interaction, which can depend on parameters such as protein type.

In another study, Matczuk et al. quantified the binding stoichiometry between AuNPs and albumin using CE-ICP-MS. Based on the initial concentrations of albumin and AuNPs and the peak area ratio of the total AuNPs to conjugated AuNPs, they calculated the binding stoichiometries for various-sized nanoparticles [90].

Legat et al. did an extension of the previous study by Matczuk et al. and compared the binding behaviors of spherical and rod-shaped AuNPs, denoted as sAuNPs and rAuNPs, respectively. Furthermore, they found the surface functionalization of

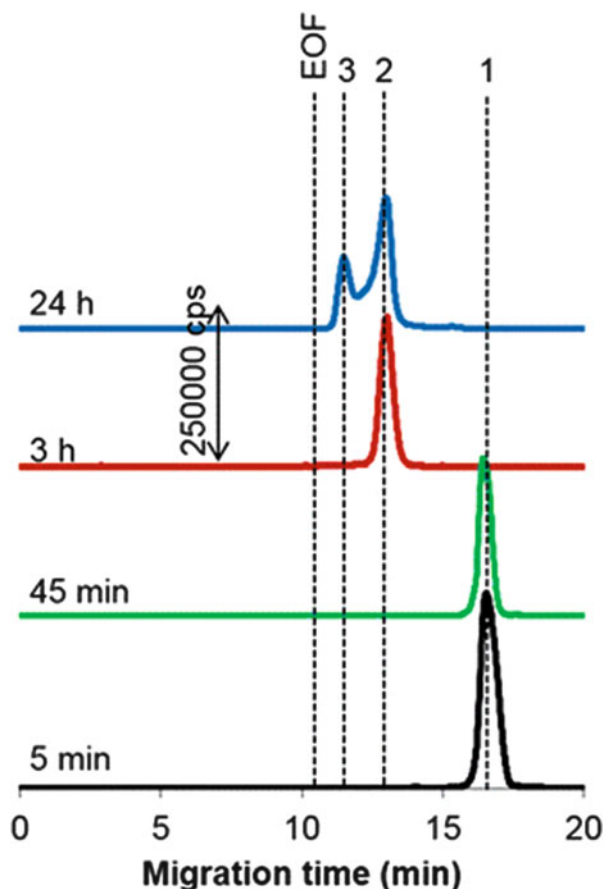
Fig. 3.10 Protein binding after incubation of 19 mg/L of 20 nm AuNPs in diluted human serum. Lines: 1 – holo-transferrin conjugate; 2 – apo-transferrin conjugate; 3 – albumin conjugate; 4 – indication of the migration time for AuNPs. (Reprinted with permission from Ref. [88]. Copyright 2015 Metallomics)



AuNPs affects the binding efficiencies to serum proteins. This work highlights the importance in the effect of AuNPs' characteristics on their functionality. Finally, they introduced sAuNPs and rAuNPs to a mixture of albumin, apo-transferrin, and holo-transferrin. sAuNPs completely changed to the conjugated form with only albumin; on the other hand, rAuNPs underwent slow association with both forms of transferrin proteins of which the apo-transferrin conjugate formed first as seen in Fig. 3.11 [91].

Boulos et al. conducted steady-state fluorescence quenching titration and ACE to extract kinetic information from the interaction between BSA and AuNPs with various surface charges. Polyacrylic acid (PAA), polyallylamine hydrochloride (PAH), and methoxy-polyethylene glycol (PEG) were the anionic, cationic, and

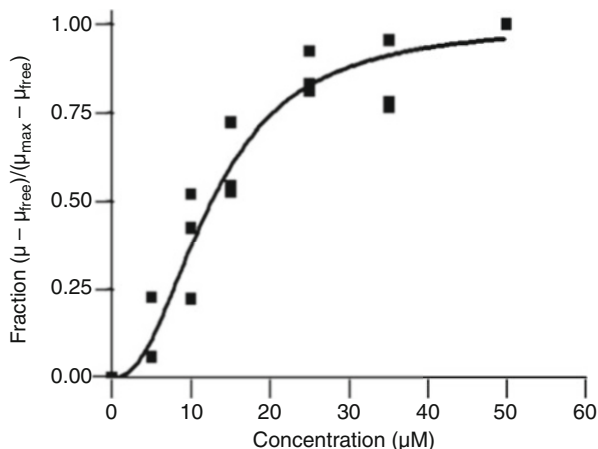
Fig. 3.11 ^{197}Au electropherograms of carboxy-rAuNPs with transferrin and albumin proteins at various incubation times. Peaks: 1 – free nanoparticles, 2 – apotransferrin conjugate, 3 – holo-transferrin conjugate. (Reprinted with permission from Ref. [91]. Copyright 2017 Chromatographia)



neutral polymer surface coatings on the AuNPs, respectively. They included BSA, which has been used as an inner wall coating in CE [92], in the background electrolyte; in effect, this reduced the EOF. By using dimethylformamide as a neutral marker, they normalized the electrophoretic mobility by EOF subtraction. Plotting the ratio of bound nanoparticle to total nanoparticle against the concentration of BSA allowed for derivation of association equilibrium constants from the Hill equation as shown in Fig. 3.12. Overall, they found that BSA adheres to PEG-functionalized AuNPs with similar affinity to charged AuNPs. Compared to the other modified AuNPs, PAH-modified AuNPs had higher affinity to BSA [93].

Nanoparticle modifications, such as those based on thiol derivatives, can improve the stability and reduce aggregation of nanoparticles [94]. López-Lorente et al. studied the effect of two thiol derivative buffer additives on the electrophoretic mobility and separation of Au and AgNPs. In their study, derivatization was performed in capillary via incorporation of thiocetic acid (TA) and thiomalic acid (TMA) in the electrophoretic buffer, which consisted of 40 mM SDS and 10 mM

Fig. 3.12 Plot of the ratio of bound nanoparticles to total nanoparticles against the concentration of BSA. The dissociation constant is calculated via the Hill equation, which was fitted to the curve plotted from pooled data. The data was obtained for PAA-GNRs with increasing concentration of BSA in 5 mM MOPS buffer. (Reprinted with permission from Ref. [93]. Copyright 2013 Langmuir)



3-(cyclohexylamino)-1-propanesulfonic acid (CAPS). The structures of the two thiol-based buffer additives are shown in Fig. 3.13. With TA in the buffer solution, the migration time of AuNPs increased; whereas, the migration time of both Au and AgNPs increased with TMA in the buffer solution as shown in the contour graph in Fig. 3.14. Furthermore, AgNPs had a higher increase in their migration time [95]. The overall structure and other functional groups of the acids seem to alter the strength of the metal-sulfur bond, especially since gold has a higher proclivity than silver to interact with H₂S [96]. The study on thiol derivative buffer additives exemplifies the applicability of CE on the characterization of nanoparticles with SAMs. Furthermore, the characterization of surface-modified nanoparticles can lead to the understanding of the potential effects of these modifications on protein adsorption.

5.2.2 Metal Oxide Nanoparticles

Metal oxide nanoparticles have been directly incorporated into drug delivery systems, and this has been studied by the use of CE to determine the delivery and encapsulation efficiencies. Doxorubicin (DOX) is a drug used in the treatment of various cancer types and the efficiency of this drug is improved by delivery in a carrier system. Gautier et al. loaded DOX-Fe²⁺ onto the surface of PEGylated superparamagnetic iron oxide nanoparticles (SPION). After analyzing the interaction and distribution of doxorubicin-loaded PEGylated SPION (DLPS) via fluorescence confocal spectral imaging (FCSI), the authors optimized the CE conditions for separation of DOX derivative molecules to overcome the challenge of differentiating chemical structure similarities. They found that modification of the capillary wall with the CEofix kitTM from Analis improved the peak shape and use of MEKC enhanced resolution. The group treated MCF-7 breast cancer cells with DOX or DLPS and obtained subcellular fractions via liquid-liquid extraction. These fractions were then analyzed by capillary electrophoresis-laser induced fluorescence (CE-LIF) to differentiate DOX and its metabolites. Along with the FCSI results, the lack of DOX metabolites detected in CE indicated that DLPS delivered DOX into the cell [97].

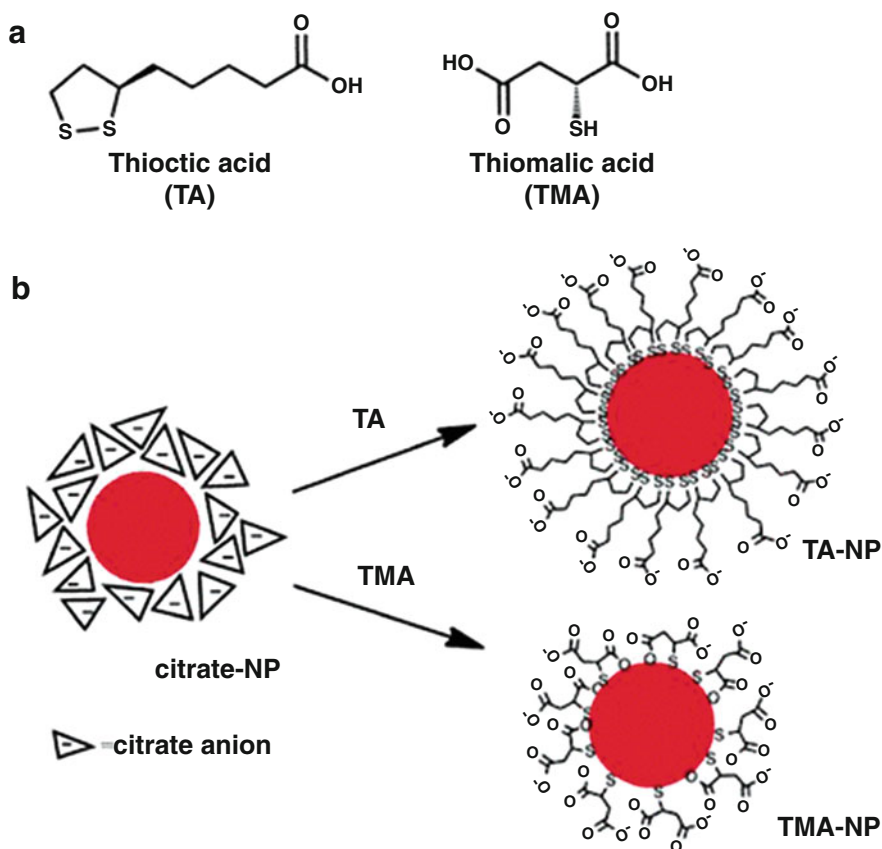


Fig. 3.13 (a) Structures of thioctic acid (TA) and thiomalic acid (TMA), which were the buffer additives used to resolve AuNPs and AgNPs. (b) Functionalization scheme for: (1) TA-NPs; (2) TMA-NPs (drawings are not to scale). (Reprinted with permission from Ref. [95]. Copyright 2014 *Microchimica Acta*)

Blazkova et al. also studied the use of DOX carriers for cancer treatment. They encapsulated DOX into apoferritin cages and conjugated this structure to magnetic nanoparticles. As shown in Fig. 3.15a, they found one peak corresponding to encapsulated DOX and the other corresponding to free DOX, which the authors attributed to the lack of success in eliminating free DOX during dialysis. The group explained that DOX molecules adhered to the surface of the apoferritin cage and were separated during electrophoresis. The correlation between the peak height and the concentration of DOX was found to be linear in Fig. 3.15b. In Fig. 3.15c, d, the amount of desorbed DOX increased while the amount of encapsulated DOX increased almost two times as much with a larger application of DOX amount. Through CE, they monitored the magnetic particle-mediated APODOX transport involving the following steps: separating the free DOX and encapsulated DOX using magnetic pull down and pH-mediated release of DOX from APODOX and APODOX-conjugated magnetic nanoparticles [98].

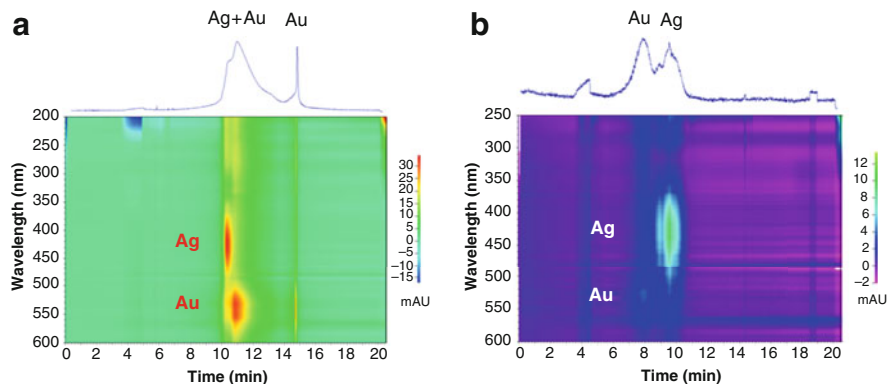


Fig. 3.14 Contour graph demonstrating the relationship between the absorbance at each wavelength and the migration time for the AuNP and AgNP mixture (a) in a buffer electrolyte with 0.1% (v/w) TA; detection wavelength at 539 nm, and (b) in a buffer electrolyte with 0.1% (v/w) of TMA; detection wavelength at 539 nm. (Reprinted with permission from Ref. [95]. Copyright 2014 Microchimica Acta)

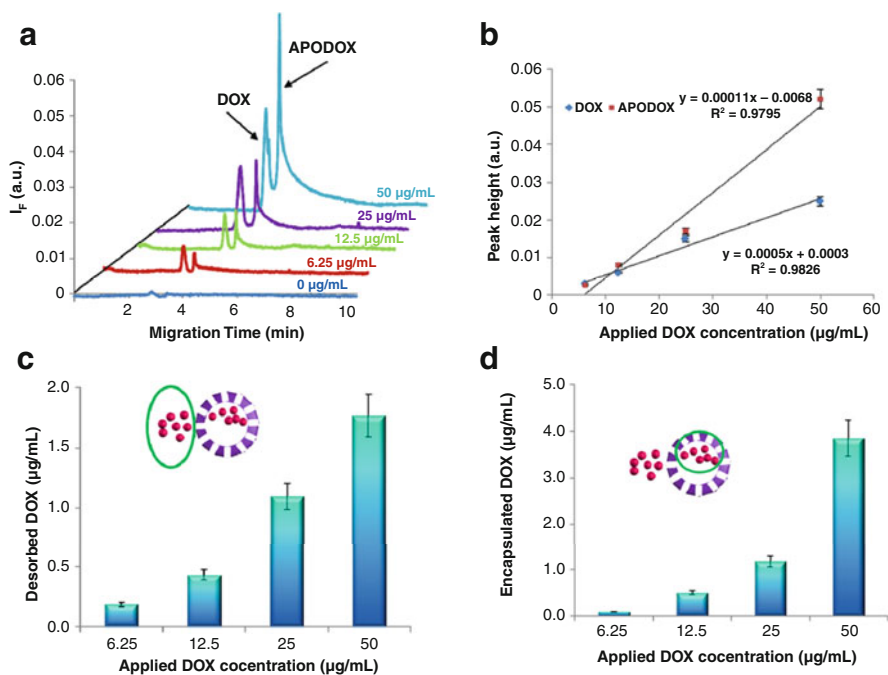


Fig. 3.15 (a) Electropherograms of APODOX solutions with the following concentrations of DOX: 0, 6.25, 12.5, 25, and 50 µg/mL. (b) Relationship between peak heights of DOX and APODOX peaks and the applied concentration of DOX. (c) Relationship between the concentration of desorbed DOX and the applied concentration of DOX. (d) Relationship between the concentration of encapsulated DOX and the applied concentration of DOX. (Reprinted with permission from Ref. [98]. Copyright 2013 International Journal of Molecular Sciences)

5.2.3 Polymeric Nanoparticles

As exemplified by the previous reports on the involvement of metal oxide nanoparticles in drug carrier systems, other literature sources assessed the usage of polymeric nanoparticles in drug delivery in addition to the study of polymeric nanoparticles and their biomolecular interactions. Oukacine et al. studied the hydrophobic properties of PEG-b-PGlu, which are the diblock copolymers that make up (1,2-diamino-cyclohexane)platinum(II) ((DACH)Pt)-loaded micelles, by using MEKC with SDS molecules in the buffer electrolyte. The electrophoretic mobility of the diblock copolymer decreases with high levels of negatively charged SDS molecules that adhere to PEG. Figure 3.16a shows the degradation of (DACH)Pt-loaded polymeric micelles, affected by a highly concentrated NaCl solution and 25 °C temperature conditions, over time. The authors observed the formation and increase of a second peak, which they suspected to be the smaller aggregates from the polymeric micelles. The peak area ratio of the degradation product to the original polymeric micelles was plotted in Fig. 3.16b [99].

Molecularly imprinted polymer nanoparticles (MIP NPs) are included in the repertoire of drug delivery tools. Although they have not been extensively studied for drug delivery purposes using CE, they have been studied for their interaction with biomolecules. Musile et al. studied the interaction of molecularly imprinted polymer nanoparticles (MIP NPs) with CE. After confirmation of the lack of MIP NPs' adsorption to the capillary wall, the group compared the interactions of MIP NPs and nonimprinted polymer nanoparticles. MIP NPs were incubated with increased concentrations of template in order for the group to obtain the binding isotherm for the complex and a dissociation equilibrium constant of $66 \pm 1 \mu\text{M}$. Selectivity was tested using angiotensin, a nonspecific ligand peptide, and it was found that there was no significant binding between MIP NPs and angiotensin [100].

Properties, such as hydrodynamic diameter and even polydispersity index, can be obtained using the theory of "Taylor dispersion," which is a result of nonuniform

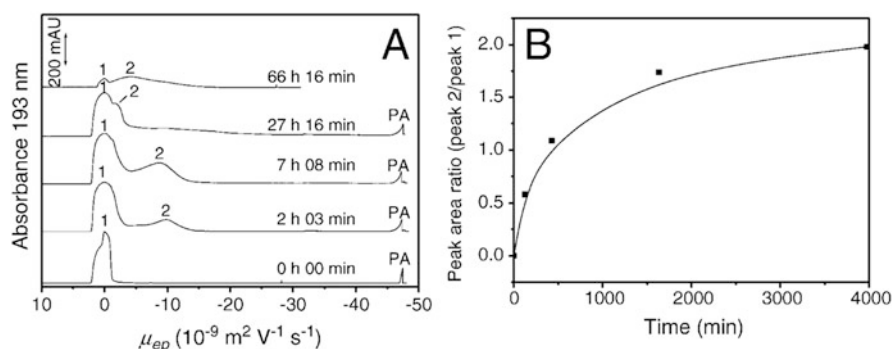


Fig. 3.16 Monitoring the decomposition of polymeric micelles in NaCl solution at 25 °C via CZE. Separation conditions: 30 mM phosphate buffer, pH 7.2, + 15 kV. Peaks: 1 – (DACH)Pt-loaded polymeric micelles; 2 – (DACH)Pt-loaded aggregates; PA phthalic acid. (Reprinted with permission from Ref. [99]. Copyright 2014 Journal of Controlled Release)

fluid velocity and molecular diffusion [101]. Ibrahim et al. used CE with Taylor Dispersion Analysis (TDA) to assess the hydrodynamic diameter and effective charge of polyglutamate backbone grafted with hydrophobic vitamin E (pGVE) hydrogels and polyglutamate (pGlu) hydrogels, which do not include vitamin E. They found a decrease in the effective charge number per nonmodified glutamate with inclusion of vitamin E in the hydrogel due to the influence of hydrophobic groups on the dissociation of glutamate molecules [102].

5.2.4 Liposomes

Liposomes can also be considered nanoparticles, and they have been a dominant option as a drug delivery tool. CE has been often used for the characterization of liposome properties, such as size, charge, and permeability, in drug delivery systems [103]. Nguyen et al. investigated PEGylated liposomes with CE-ICP-MS for the use of cisplatin anti-cancer drug delivery. They were able to separate liposome-encapsulated cisplatin from free cisplatin and hydrolysis products of cisplatin in human plasma. Coupling CE to ICP-MS allowed for simultaneous monitoring of phosphorus from phospholipids and platinum from cisplatin. Increasing the plasma amount caused a decrease in the signal of cisplatin; in addition, cisplatin and hydrolysis products co-migrated as one peak when the matrix was 50% plasma. They found that reducing the plasma amount to 20% was necessary to improve resolution and sensitivity during separation. The group speculated that the addition of SDS to the background electrolyte improved separation efficiency possibly due to the surfactant reducing adsorption to the capillary wall [104].

Nguyen et al. also studied the release of cisplatin from liposomes, which was induced by sonication. Based on reduction of peaks for free cisplatin and hydrolysis products, the amount of release cisplatin was calculated [105]. Otarola et al. analyzed the entrapment efficiency of their prepared nanostructured lipid carrier (NLC) with incorporated piroxicam, a nonsteroidal anti-inflammatory drug (NSAID) using CE. They obtained the entrapment efficiency by calculating the difference between the amount of piroxicam used for NLC suspensions and the amount of piroxicam not entrapped in the NLCs [106].

5.2.5 Quantum Dots

In general, quantum dots have been important tools for drug delivery, bioimaging, and sensors. In CE, they have been conjugated with biomolecules in interaction and detection studies. Janu et al. capped CdTe-QDs with heptapeptides (HWRGWVC) to conjugate to human immunoglobulin. They observed that HWR peptide has affinity towards IgG but not IgY. The IgG complex was separated from the IgY complex as well as the HWR peptide-capped QDs. HWR-QD conjugation was confirmed by magnetic particles coated with IgG and IgY in differential pulse voltammograms. The same binding phenomenon occurred in gel electrophoresis and ELISA results as well [107].

Zhou et al. also used quantum dots in a capillary electrophoresis-chemiluminescence (CE-CL) detection system, but their goal was to detect the presence of carcinoembryonic antigen (CEA) with their method. Their HRP-DNA_{A-B}-QD probe

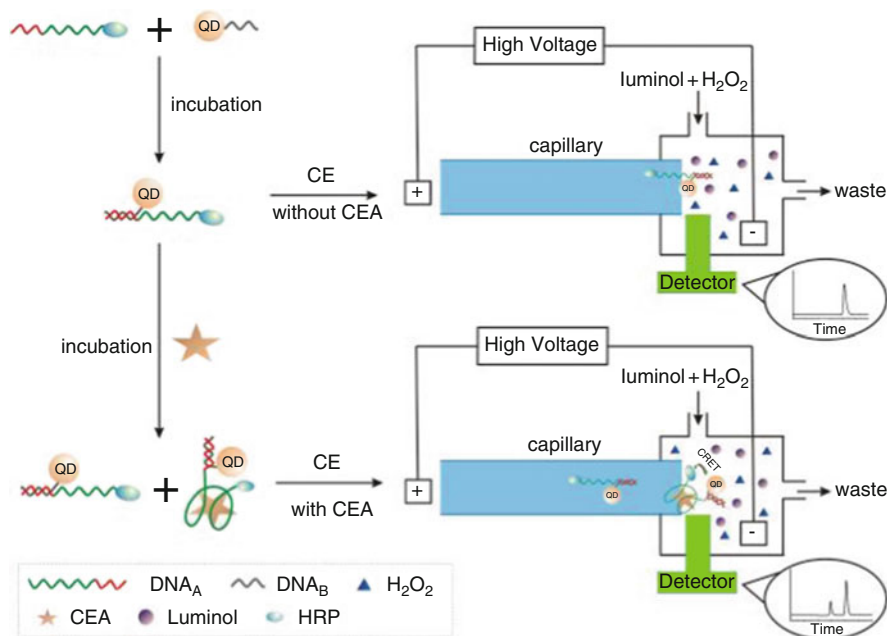


Fig. 3.17 Detection of CEA antigen with an aptamer-labeled QD probe by CE-CL detection system. CEA-probe complex can be separated from the free probe. (Reprinted with permission from Ref. [108]. Copyright 2015 Sensors and Actuators B: Chemical)

was designed to enable chemiluminescence resonance energy transfer (CRET) when bound to the target antigen. With CEA in the mixture, the CEA/HRP-DNA_{A-B}-QD complex was present and could be separated from the free probe in CE, as shown in Fig. 3.17. When compared to the calibration values for quantification of CEA in human serum by the standard LIAISON chemiluminescence immunoassay system, the authors' results from using their probe combined with the CE-CL detection system were similar [108].

6 Conclusions and Future Perspective

Open channel separation including FFF and CE are unique approaches for the study of nanomaterials and their bioconjugates as well as their application to drug delivery systems. They provide fast separation and sufficient resolution between the non-conjugated and conjugated nanomaterials for rapid characterization of the nanomaterial itself and biological layer formation. The different separation modes in each technique also provide superior tools for analysis of different physicochemical properties of the nanomaterials, including size, shape, and surface potential. Still, there is a deficiency in applications on the newer generation of nanomaterials, the 1D and 2D materials, like fibers and sheets. Lack of theory to guide separation optimization of

such materials is the main challenge behind this gap. In addition, hyphenation with more detectors or other separation techniques are desired to improve the amounts of information obtained upon separation. Sample throughput and collection recovery are to be improved for FFF, which is more prominent in recovering samples for down-stream analysis than CE. However, with the advancement in the instrumentation of CE-MS, more applications in this area are to be expected. Moreover, the previous efforts are all focused on protein conjugates. Future applications on analyzing adsorption of other biomolecules, like nucleic acids and lipids, are expected to explore contribution of other adsorbed or conjugated biomolecules on nanomaterials that could alter their biological behaviors. In addition, more analysis on drug delivery systems using open channel separation is a possibility, and potential avenues include studies with other nanomaterial types aside from polymeric and lipid-based ones, which have been dominant in FFF and CE research. Overall, while open channel separation techniques have shown strong power in the study of nanomaterials, more instrumentation developments and wider application scopes are expected in the coming years to improve their capability in characterization of diverse new nanomaterials and their bioconjugates and to meet the accompanying challenges in the fast development of nanotechnology.

Acknowledgments The authors thank the support from the National Institute of Environmental Health Sciences of the National Institutes of Health under the Award #U01ES027293 (to W. Z.) and T32ES018827 (to R. C.).

References

1. Kim S, Lim YT, Soltesz EG, De Grand AM, Lee J, Nakayama A, Parker JA, Mihaljevic T, Laurence RG, Dor DM, Cohn LH, Bawendi MG, Frangioni JV (2004) Near-infrared fluorescent type II quantum dots for sentinel lymph node mapping. *Nat Biotechnol* 22:93–97. <https://doi.org/10.1038/nbt920>
2. So M-K, Xu C, Loening AM, Gambhur SS, Rao J (2006) Self-illuminating quantum dots aid in vivo imaging. *Nat Biotechnol* 24:339–343. <https://doi.org/10.1038/nbt1188>
3. Yu MK, Jeong YY, Park J, Park S, Kim JW, Min JJ, Kim K, Jon S (2008) Drug-loaded superparamagnetic iron oxide nanoparticles for combined cancer imaging and therapy in vivo. *Angew Chemie – Int Ed* 47:5362–5365. <https://doi.org/10.1002/anie.200800857>
4. Alexiou C, Arnold W, Klein RJ, Parak FG, Hulin P, Bergemann C, Erhardt W, Wagenpfeil S, Lübke AS (2000) Locoregional cancer treatment with magnetic drug targeting. *Cancer Res* 60:6641–6648
5. Wang Y, Sun Y, Wang J, Yang Y, Li Y, Yuan Y, Liu C (2016) Charge-reversal APTES-modified mesoporous silica nanoparticles with high drug loading and release controllability. *ACS Appl Mater Interfaces* 8:17166–17175. <https://doi.org/10.1021/acsami.6b05370>
6. Zhang CY, Yeh HC, Kuroki MT, Wang TH (2005) Single-quantum-dot-based DNA nanosensor. *Nat Mater* 4:826–831. <https://doi.org/10.1038/nmat1508>
7. Lundqvist M, Stigler J, Elia G, Lynch I, Cedervall T, Dawson KA (2008) Nanoparticle size and surface properties determine the protein corona with possible implications for biological impacts. *Proc Natl Acad Sci* 105:14265–14270. <https://doi.org/10.1073/pnas.0805135105>
8. Tenzer S, Docter D, Kuharev J, Musyanovych A, Fetz V, Hecht R, Schlenk F, Fischer D, Kiouptsi K, Reinhardt C, Landfester K, Schild H, Maskos M, Knauer SK, Stauber RH (2013)

- Rapid formation of plasma protein corona critically affects nanoparticle pathophysiology. *Nat Nanotechnol* 8:772–781. <https://doi.org/10.1038/nnano.2013.181>
9. An H, Jin B (2012) Prospects of nanoparticle-DNA binding and its implications in medical biotechnology. *Biotechnol Adv* 30:1721–1732. <https://doi.org/10.1016/j.biotechadv.2012.03.007>
 10. Villanueva A, Cañete M, Roca AG, Calero M, Veintemillas-Verdaguer S, Serna CJ, del Puerto Morales M, Miranda R (2009) The influence of surface functionalization on the enhanced internalization of magnetic nanoparticles in cancer cells. *Nanotechnology* 20:115103. <https://doi.org/10.1088/0957-4484/20/11/115103>
 11. Westmeier D, Stauber RH, Docter D (2016) The concept of bio-corona in modulating the toxicity of engineered nanomaterials (ENM). *Toxicol Appl Pharmacol* 299:53–57. <https://doi.org/10.1016/j.taap.2015.11.008>
 12. Wang F, Yu L, Monopoli MP, Sandin P, Mahon E, Salvati A, Dawson KA (2013) The biomolecular corona is retained during nanoparticle uptake and protects the cells from the damage induced by cationic nanoparticles until degraded in the lysosomes. *Nanomed Nanotechnol Biol Med* 9:1159–1168. <https://doi.org/10.1016/j.nano.2013.04.010>
 13. Ke PC, Lin S, Parak WJ, Davis TP, Caruso F (2017) A decade of the protein corona. *ACS Nano* 11:11773
 14. Cedervall T, Lynch I, Lindman S, Berggard T, Thulin E, Nilsson H, Dawson KA, Linse S (2007) Understanding the nanoparticle-protein corona using methods to quantify exchange rates and affinities of proteins for nanoparticles. *Proc Natl Acad Sci* 104:2050–2055. <https://doi.org/10.1073/pnas.0608582104>
 15. Ulbrich K, Holá K, Šubr V, Bakandritsos A, Tuček J, Zbořil R (2016) Targeted drug delivery with polymers and magnetic nanoparticles: covalent and noncovalent approaches, release control, and clinical studies. *Chem Rev* 116:5338–5431. <https://doi.org/10.1021/acs.chemrev.5b00589>
 16. Filipe V, Hawe A, Jiskoot W (2010) Critical evaluation of nanoparticle tracking analysis (NTA) by NanoSight for the measurement of nanoparticles and protein aggregates. *Pharm Res* 27:796–810. <https://doi.org/10.1007/s11095-010-0073-2>
 17. Wei GT, Liu F-K, Wang CRC (1999) Shape separation of nanometer gold particles by size-exclusion chromatography. *Anal Chem* 71:2085–2091. <https://doi.org/10.1021/ac990044u>
 18. Wilcoxon JP, Martin JE, Provencio P (2000) Size distributions of gold nanoclusters studied by liquid chromatography. *Langmuir* 16:9912–9920. <https://doi.org/10.1021/la000669j>
 19. Hanauer M, Pierrat S, Zins I, Lotz A, Sönnichsen C (2007) Separation of nanoparticles by gel electrophoresis according to size and shape. *Nano Lett* 7:2881–2885. <https://doi.org/10.1021/nl071615y>
 20. Xu X, Caswell KK, Tucker E, Kabisatpathy S, Brodhacker KL, Scrivens WA (2007) Size and shape separation of gold nanoparticles with preparative gel electrophoresis. *J Chromatogr A* 1167:35–41. <https://doi.org/10.1016/j.chroma.2007.07.056>
 21. Giddings JC (1966) A new separation concept based on a coupling of concentration and flow nonuniformities. *Sep Sci* 1:123–125. <https://doi.org/10.1080/01496396608049439>. Published
 22. Giddings JC (1993) Field-flow fractionation – analysis of macromolecular, colloidal, and particulate materials. *Science* (80-) 260:1456–1465. <https://doi.org/10.1126/science.8502990>
 23. Liu MK, Li P, Giddings JC (1993) Rapid protein separation and diffusion coefficient measurement by frit inlet flow field-flow fractionation. *Protein Sci* 2:1520–1531. <https://doi.org/10.1002/pro.5560020917>
 24. Giddings JC, Yang FJ, Myers MN (1977) Flow field-flow fractionation as a methodology for protein separation and characterization. *Anal Biochem* 81:395–407. [https://doi.org/10.1016/0003-2697\(77\)90710-2](https://doi.org/10.1016/0003-2697(77)90710-2)
 25. Liu MK, Giddings JC (1993) Separation and measurement of diffusion coefficients of linear and circular DNAs by flow field-flow fractionation. *Macromolecules* 26:3576–3588. <https://doi.org/10.1021/ma00066a016>
 26. Ashby J, Schachermeyer S, Duan Y, Jimenez LA, Zhong W (2014) Probing and quantifying DNA-protein interactions with asymmetrical flow field-flow fractionation. *J Chromatogr A* 1358:217–224. <https://doi.org/10.1016/j.chroma.2014.07.002>

27. Bousse T, Shore DA, Goldsmith CS, Hossain MJ, Jang Y, Davis CT, Donis RO, Stevens J (2013) Quantitation of influenza virus using field flow fractionation and multi-angle light scattering for quantifying influenza A particles. *J Virol Methods* 193:589–596. <https://doi.org/10.1016/j.jviromet.2013.07.026>
28. Giddings JC, Yang FJ, Myers MN (1977) Flow field-flow fractionation – new method for separating, purifying, and characterizing diffusivity of viruses. *J Virol* 21:131–138. <https://doi.org/10.1007/s11664-014-3204-4>
29. Flack K, Jimenez LA, Zhong W (2017) Analysis of the distribution profiles of circulating microRNAs by asymmetrical flow field flow fractionation. In: Rani S. (eds) *MicroRNA profiling. Methods in molecular biology*, vol 1509. Humana Press, New York, NY, pp 161–168
30. Wagner M, Pietsch C, Tauhardt L, Schallon A, Schubert US (2014) Characterization of cationic polymers by asymmetric flow field-flow fractionation and multi-angle light scattering—a comparison with traditional techniques. *J Chromatogr A* 1325:195–203. <https://doi.org/10.1016/j.chroma.2013.11.049>
31. Giddings JC (1973) The conceptual basis of field-flow fractionation. *J Chem Educ* 50:667. <https://doi.org/10.1021/ed050p667>
32. Kowalkowski T, Buszewski B, Cantado C, Dondi F (2006) Field-flow fractionation: theory, techniques, applications and the challenges. *Crit Rev Anal Chem* 36:129–135. <https://doi.org/10.1080/10408340600713702>
33. Contado C (2017) Field flow fractionation techniques to explore the “nano-world”. *Anal Bioanal Chem* 409:2501–2518. <https://doi.org/10.1007/s00216-017-0180-6>
34. Bednar AJ, Poda AR, Mitrano DM, Kennedy AJ, Gray EP, Ranville JF, Hayes CA, Crocker FH, Steevens JA (2013) Comparison of on-line detectors for field flow fractionation analysis of nanomaterials. *Talanta* 104:140–148. <https://doi.org/10.1016/j.talanta.2012.11.008>
35. Schachermeyer S, Ashby J, Zhong W (2012) Advances in field-flow fractionation for the analysis of biomolecules: instrument design and hyphenation. *Anal Bioanal Chem* 404:1151–1158. <https://doi.org/10.1007/s00216-012-6069-5>
36. Szolar OHJ, Brown RS, Luong JHT (1995) Separation of PAHs by capillary electrophoresis with laser-induced fluorescence detection using mixtures of neutral and Anionic.β-cyclodextrins. *Anal Chem* 67:3004–3010. <https://doi.org/10.1021/ac00113a039>
37. Cheng HL, Liao YM, Chiou SS, Wu SW (2008) On-line stacking capillary electrophoresis for analysis of methotrexate and its eight metabolites in whole blood. *Electrophoresis* 29:3665–3673. <https://doi.org/10.1002/elps.200800029>
38. Sun L, Zhu G, Zhang Z, Mou S, Dovichi NJ (2015) Third-generation electrokinetically pumped sheath-flow nanospray interface with improved stability and sensitivity for automated capillary zone electrophoresis-mass spectrometry analysis of complex proteome digests. *J Proteome Res* 14:2312–2321. <https://doi.org/10.1021/acs.jproteome.5b00100>
39. Han F, Huynh BH, Ma Y, Lin B (1999) High-efficiency DNA separation by capillary electrophoresis in a polymer solution with ultralow viscosity. *Anal Chem* 71:2385–2389. <https://doi.org/10.1097/JCP.0b013e3182549d2d>
40. Nehme H, Nehme R, Lafite P, Routier S, Morin P (2012) New development in in-capillary electrophoresis techniques for kinetic and inhibition study of enzymes. *Anal Chim Acta* 722:127–135. <https://doi.org/10.1016/j.aca.2012.02.003>
41. Mattarozzi M, Suman M, Cascio C, Calestani D, Weigel S, Undas A, Peters R (2017) Analytical approaches for the characterization and quantification of nanoparticles in food and beverages. *Anal Bioanal Chem* 409:63–80. <https://doi.org/10.1007/s00216-016-9946-5>
42. Bandyopadhyay S, Peralta-Videa JR, Gardea-Torresdey JL (2013) Advanced analytical techniques for the measurement of nanomaterials in complex samples: a comparison. *Environ Eng Sci* 30:118–125. <https://doi.org/10.3920/QAS2014.0410>
43. Sadik OA, Du N, Kariuki V, Okello V, Bushlyar V (2014) Current and emerging technologies for the characterization of nanomaterials. *ACS Sustain Chem Eng* 2:1707–1716. <https://doi.org/10.1021/sc500175v>

44. Meermann B, Laborda F (2015) Analysis of nanomaterials by field-flow fractionation and single particle ICP-MS. *J Anal At Spectrom* 30:1226–1228. <https://doi.org/10.1039/c5ja90019k>
45. Chetwynd A, Guggenheim E, Briffa S, Thorn J, Lynch I, Valsami-Jones E (2018) Current application of capillary electrophoresis in nanomaterial characterisation and its potential to characterise the protein and small molecule corona. *Nanomaterials* 8. <https://doi.org/10.3390/nano8020099>
46. Yohannes G, Jussila M, Hartonen K, Riekkola ML (2011) Asymmetrical flow field-flow fractionation technique for separation and characterization of biopolymers and bioparticles. *J Chromatogr A* 1218:4104–4116. <https://doi.org/10.1016/j.chroma.2010.12.110>
47. Giddings JC, Yang FJF, Myers MN (1976) Flow field-flow fractionation: a versatile new separation method. *Science* (80-) 193:1244–1245
48. Mudalige TK, Qu H, Sánchez-Pomales G, Sisco PN, Linder SW (2015) Simple functionalization strategies for enhancing nanoparticle separation and recovery with asymmetric flow field flow fractionation. *Anal Chem* 87:1764–1772. <https://doi.org/10.1021/ac503683n>
49. Rambaldi DC, Reschiglian P, Zattoni A (2011) Flow field-flow fractionation: recent trends in protein analysis. *Anal Bioanal Chem* 399:1439–1447. <https://doi.org/10.1007/s00216-010-4312-5>
50. Wahlund KG, Giddings JC (1987) Properties of an asymmetrical flow field-flow fractionation channel having one permeable wall. *Anal Chem* 59:1332–1339. <https://doi.org/10.1021/ac00136a016>
51. Mudalige TK, Qu H, Van Haute D, Ansar SM, Linder SW (2018) Capillary electrophoresis and asymmetric flow field-flow fractionation for size-based separation of engineered metallic nanoparticles: a critical comparative review. *TrAC – Trends Anal Chem* 106:202–212. <https://doi.org/10.1016/j.trac.2018.07.008>
52. Schachermeyer S, Ashby J, Kwon M, Zhong W (2012) Impact of carrier fluid composition on recovery of nanoparticles and proteins in flow field flow fractionation. *J Chromatogr A* 1264:72–79. <https://doi.org/10.1016/j.chroma.2012.09.050>
53. Ashby J, Schachermeyer S, Pan S, Zhong W (2013) Dissociation-based screening of nanoparticle-protein interaction via flow field-flow fractionation. *Anal Chem* 85:7494–7501. <https://doi.org/10.1021/ac401485j>
54. Ashby J, Flack K, Jimenez LA, Duan Y, Khatib AK, Somlo G, Wang SE, Cui X, Zhong W (2014) Distribution profiling of circulating MicroRNAs in serum. *Anal Chem* 86:9343–9349. <https://doi.org/10.1021/ac5028929>
55. Chu YH, Avila LZ, Biebuyck HA, Whitesides GM (1992) Use of affinity capillary electrophoresis to measure binding constants of ligands to proteins. *J Med Chem* 35:2915–2917. <https://doi.org/10.1021/jm00093a027>
56. Chu Y-H, Avila LZ, Gao J, Whitesides GM (1995) Affinity capillary electrophoresis. *Acc Chem Res* 28:461–468. <https://doi.org/10.1021/ar00059a004>
57. Li N, Zeng S, He L, Zhong W (2010) Probing nanoparticle– protein interaction by capillary electrophoresis. *Anal Chem* 82:7460–7466
58. Terabe S, Otsuka K, Ichikawa K, Tsuchiya A, Ando T (1984) Electrokinetic separations with micellar solutions and open-tubular capillaries. *Anal Chem* 56:111–113. <https://doi.org/10.1021/ac00265a031>
59. Liu FK, Wei GT (2004) Adding sodium dodecylsulfate to the running electrolyte enhances the separation of gold nanoparticles by capillary electrophoresis. *Anal Chim Acta* 510:77–83. <https://doi.org/10.1016/j.aca.2003.12.064>
60. Ciriello R, Ialorenzi PT, Laurita A, Guerrieri A (2017) Improved separation and size characterization of gold nanoparticles through a novel capillary zone electrophoresis method using poly(sodium4-styrenesulfonate) as stabiliser and a stepwise field strength gradient. *Electrophoresis* 38:922–929. <https://doi.org/10.1002/elps.201600478>
61. Kairdolf BA, Qian X, Nie S (2017) Bioconjugated nanoparticles for biosensing, in vivo imaging, and medical diagnostics. *Anal Chem* 89:1015–1031. <https://doi.org/10.1021/acs.analchem.6b04873>

62. Bazak R, Hourri M, El Achy S, Kamel S, Refaat T (2015) Cancer active targeting by nanoparticles: a comprehensive review of literature. *J Cancer Res Clin Oncol* 141:769–784. <https://doi.org/10.1007/s00432-014-1767-3>
63. Hizir MS, Top M, Balcioglu M, Rana M, Robertson NM, Shen F, Sheng J, Yigit MV (2016) Multiplexed activity of perAoxidase: DNA-capped AuNPs act as adjustable peroxidase. *Anal Chem* 88:600–605. <https://doi.org/10.1021/acs.analchem.5b03926>
64. Li H, Shen J, Cui R, Sun C, Zhao Y, Wu X, Li N, Tang B (2017) A highly selective and sensitive fluorescent nanosensor for dopamine based on formate bridged Tb(iii) complex and silver nanoparticles. *Analyst* 142:4240–4246. <https://doi.org/10.1039/c7an00961e>
65. Safenkova IV, Slutskaya ES, Panferov VG, Zherdev AV, Dzantiev BB (2016) Complex analysis of concentrated antibody-gold nanoparticle conjugates' mixtures using asymmetric flow field-flow fractionation. *J Chromatogr A* 1477:56–63. <https://doi.org/10.1016/j.chroma.2016.11.040>
66. Poda AR, Bednar AJ, Kennedy AJ, Harmon A, Hull M, Mitrano DM, Ranville JF, Steevens J (2011) Characterization of silver nanoparticles using flow-field flow fractionation interfaced to inductively coupled plasma mass spectrometry. *J Chromatogr A* 1218:4219–4225. <https://doi.org/10.1016/j.chroma.2010.12.076>
67. Tadjiki S, Montaño MD, Assemi S, Barber A, Ranville J, Beckett R (2017) Measurement of the density of engineered silver nanoparticles using centrifugal FFF-TEM and single particle ICP-MS. *Anal Chem* 89:6056–6064. <https://doi.org/10.1021/acs.analchem.7b00652>
68. Marassi V, Roda B, Casolari S, Ortelli S, Blosi M, Zattoni A, Costa AL, Reschiglian P (2018) Hollow-fiber flow field-flow fractionation and multi-angle light scattering as a new analytical solution for quality control in pharmaceutical nanotechnology. *Microchem J* 136:149–156. <https://doi.org/10.1016/j.microc.2016.12.015>
69. Marassi V, Casolari S, Roda B, Zattoni A, Reschiglian P, Panzavolta S, Tofail SAM, Ortelli S, Delpivo C, Blosi M, Costa AL (2015) Hollow-fiber flow field-flow fractionation and multi-angle light scattering investigation of the size, shape and metal-release of silver nanoparticles in aqueous medium for nano-risk assessment. *J Pharm Biomed Anal* 106:92–99. <https://doi.org/10.1016/j.jpba.2014.11.031>
70. Wimuktiwan P, Shiowatana J, Siripinyanond A (2015) Investigation of silver nanoparticles and plasma protein association using flow field-flow fractionation coupled with inductively coupled plasma mass spectrometry (FIFFF-ICP-MS). *J Anal At Spectrom* 30:245–253. <https://doi.org/10.1039/c4ja00225c>
71. Yu B, Zhou Y, Song M, Xue Y, Cai N, Luo X, Long S, Zhang H, Yu F (2016) Synthesis of selenium nanoparticles with mesoporous silica drug-carrier shell for programmed responsive tumor targeted synergistic therapy. *RSC Adv* 6:2171–2175. <https://doi.org/10.1039/c5ra21460b>
72. Zheng S, Li X, Zhang Y, Xie Q, Wong YS, Zheng W, Chen T (2012) PEG-nanolized ultrasmall selenium nanoparticles overcome drug resistance in hepatocellular carcinoma HepG2 cells through induction of mitochondria dysfunction. *Int J Nanomedicine* 7:3939–3949. <https://doi.org/10.2147/IJN.S30940>
73. M-M P, Somchue W, Shiowatana J, Siripinyanond A (2014) Flow field-flow fractionation for particle size characterization of selenium nanoparticles incubated in gastrointestinal conditions. *Food Res Int* 57:208–209. <https://doi.org/10.1016/j.foodres.2014.01.040>
74. Seabra A, Durán N (2015) Nanotoxicology of metal oxide nanoparticles. *Metals (Basel)* 5:934–975. <https://doi.org/10.3390/met5020934>
75. Peng N, Wu B, Wang L, He W, Ai Z, Zhang X, Wang Y, Fan L, Ye Q (2016) High drug loading and pH-responsive targeted nanocarriers from alginate-modified SPIONs for anti-tumor chemotherapy. *Biomater Sci* 4:1802–1813. <https://doi.org/10.1039/c6bm00504g>
76. Martínez-Carmona M, Gun'ko Y, Vallet-Regí M (2018) ZnO nanostructures for drug delivery and theranostic applications. *Nanomaterials* 8. <https://doi.org/10.3390/nano8040268>
77. Bogdan J, Plawinska-Czarnak J, Zarzynska J (2017) Nanoparticles of titanium and zinc oxides as novel agents in tumor treatment: a review Janusz. *Nanoscale Res Lett* 12:225. <https://doi.org/10.1186/s11671-017-2007-y>

78. Ashby J, Pan S, Zhong W (2014) Size and surface functionalization of iron oxide nanoparticles influence the composition and dynamic nature of their protein corona. *ACS Appl Mater Interfaces* 6:15412–15419. <https://doi.org/10.1021/am503909q>
79. Weber C, Simon J, Mailänder V, Morsbach S, Landfester K (2018) Preservation of the soft protein corona in distinct flow allows identification of weakly bound proteins. *Acta Biomater* 76:217–224. <https://doi.org/10.1016/j.actbio.2018.05.057>
80. Wang S, McGuirk CM, d’Aquino A, Mason JA, Mirkin CA (2018) Metal-organic framework nanoparticles. *Adv Mater* 30:1800202. <https://doi.org/10.1002/adma.201800202>
81. Roda B, Marassi V, Zattoni A, Borghi F, Anand R, Agostoni V, Gref R, Reschiglian P, Monti S (2018) Flow field-flow fractionation and multi-angle light scattering as a powerful tool for the characterization and stability evaluation of drug-loaded metal-organic framework nanoparticles. *Anal Bioanal Chem* 410:5245–5253. <https://doi.org/10.1007/s00216-018-1176-6>
82. Hinna AH, Hupfeld S, Kuntsche J, Brandl M (2016) The use of asymmetrical flow field-flow fractionation with on-line detection in the study of drug retention within liposomal nano-carriers and drug transfer kinetics. *J Pharm Biomed Anal* 124:157–163. <https://doi.org/10.1016/j.jpba.2016.02.037>
83. Elgqvist J, Frost S, Pouget J-P, Albertsson P (2014) The potential and hurdles of targeted alpha therapy – clinical trials and beyond. *Front Oncol* 3:1–9. <https://doi.org/10.3389/fonc.2013.00324>
84. Huclier-Markai S, Grivaud-Le Du A, N’tsiba E, Montavon G, Mougin-Degraef M, Barbet J (2018) Coupling a gamma-ray detector with asymmetrical flow field flow fractionation (AF4): application to a drug-delivery system for alpha-therapy. *J Chromatogr A* 1573:107–114. <https://doi.org/10.1016/j.chroma.2018.08.065>
85. Moquin A, Neibert KD, Maysinger D, Winnik FM (2015) Quantum dot agglomerates in biological media and their characterization by asymmetrical flow field-flow fractionation. *Eur J Pharm Biopharm* 89:290–299. <https://doi.org/10.1016/j.ejpb.2014.12.019>
86. Bouzas-Ramos D, García-Cortes M, Sanz-Medel A, Encinar JR, Costa-Fernández JM (2017) Assessment of the removal of side nanoparticulated populations generated during one-pot synthesis by asymmetric flow field-flow fractionation coupled to elemental mass spectrometry. *J Chromatogr A* 1519:156–161. <https://doi.org/10.1016/j.chroma.2017.08.068>
87. Menéndez-Miranda M, Encinar JR, Costa-Fernández JM, Sanz-Medel A (2015) Asymmetric flow field-flow fractionation coupled to inductively coupled plasma mass spectrometry for the quantification of quantum dots bioconjugation efficiency. *J Chromatogr A* 1422:247–252. <https://doi.org/10.1016/j.chroma.2015.10.012>
88. Matczuk M, Anecka K, Scaletti F, Messori L, Keppler BK, Timerbaev AR, Jarosz M (2015) Speciation of metal-based nanomaterials in human serum characterized by capillary electrophoresis coupled to ICP-MS: a case study of gold nanoparticles. *Metallomics* 7:1364–1370. <https://doi.org/10.1039/c5mt00109a>
89. Belder D, Deege A, Husmann H, Kohler F, Ludwig M (2001) Cross-linked poly(vinyl alcohol) as permanent hydrophilic column coating for capillary electrophoresis. *Electrophoresis* 22:3813–3818. [https://doi.org/10.1002/1522-2683\(200109\)22:17<3813::AID-ELPS3813>3.0.CO;2-D](https://doi.org/10.1002/1522-2683(200109)22:17<3813::AID-ELPS3813>3.0.CO;2-D)
90. Matczuk M, Legat J, Shtykov SN, Jarosz M, Timerbaev AR (2016) Characterization of the protein corona of gold nanoparticles by an advanced treatment of CE-ICP-MS data. *Electrophoresis* 37:2257–2259. <https://doi.org/10.1002/elps.201600152>
91. Legat J, Matczuk M, Scaletti F, Messori L, Timerbaev A, Jarosz M (2017) Erratum to: CE separation and ICP-MS detection of gold nanoparticles and their protein conjugates. *Chromatographia* 80:1719. <https://doi.org/10.1007/s10337-017-3410-3>
92. Man Y, Lv X, Iqbal J, Jia F, Xiao P, Hasan M, Li Q, Dai R, Geng L, Qing H, Deng Y (2013) Adsorptive BSA coating method for CE to separate basic proteins. *Chromatographia* 76:59–65. <https://doi.org/10.1007/s10337-012-2337-y>
93. Boulos SP, Davis TA, Yang JA, Lohse SE, Alkilany AM, Holland LA, Murphy CJ (2013) Nanoparticle-protein interactions: a thermodynamic and kinetic study of the adsorption of bovine serum albumin to gold nanoparticle surfaces. *Langmuir* 29:14984–14996. <https://doi.org/10.1021/la402920f>

94. Gao J, Huang X, Liu H, Zan F, Ren J (2012) Colloidal stability of gold nanoparticles modified with thiol compounds: bioconjugation and application in cancer cell imaging. *Langmuir* 28:4464–4471. <https://doi.org/10.1021/la204289k>
95. López-Lorente ÁI, Soriano ML, Valcárcel M (2014) Analysis of citrate-capped gold and silver nanoparticles by thiol ligand exchange capillary electrophoresis. *Microchim Acta* 181:1789–1796. <https://doi.org/10.1007/s00604-014-1218-5>
96. Pakiari AH, Jamshidi Z (2010) Nature and strength of M-S bonds (M = Au, Ag, and Cu) in binary alloy gold clusters. *J Phys Chem A* 114:9212–9221
97. Gautier J, Munnier E, Soucé M, Chourpa I, Douziech Eyrolles L (2015) Analysis of doxorubicin distribution in MCF-7 cells treated with drug-loaded nanoparticles by combination of two fluorescence-based techniques, confocal spectral imaging and capillary electrophoresis. *Anal Bioanal Chem* 407:3425–3435. <https://doi.org/10.1007/s00216-015-8566-9>
98. Blazkova I, Nguyen HV, Dostalova S, Kopel P, Stanisavljevic M, Vaculovicova M, Stiborova M, Eckschlagler T, Kizek R, Adam V (2013) Apoferritin modified magnetic particles as doxorubicin carriers for anticancer drug delivery. *Int J Mol Sci* 14:13391–13402. <https://doi.org/10.3390/ijms140713391>
99. Oukacine F, Bernard S, Bobe I, Cottet H (2014) Physico-chemical characterization of polymeric micelles loaded with platinum derivatives by capillary electrophoresis and related methods. *J Control Release* 196:139–145. <https://doi.org/10.1016/j.jconrel.2014.09.022>
100. Musile G, Cenci L, Andreetto E, Ambrosi E, Tagliaro F, Bossi AM (2016) Screening of the binding properties of molecularly imprinted nanoparticles via capillary electrophoresis. *Anal Bioanal Chem* 408:3435–3443. <https://doi.org/10.1007/s00216-016-9418-y>
101. Taylor G (1953) Dispersion of soluble matter in solvent flowing slowly through a tube. *Proc R Soc A Math Phys Eng Sci* 219:186–203. <https://doi.org/10.1098/rspa.1953.0139>
102. Ibrahim A, Meyrueix R, Pouliquen G, Chan YP, Cottet H (2013) Size and charge characterization of polymeric drug delivery systems by Taylor dispersion analysis and capillary electrophoresis. *Anal Bioanal Chem* 405:5369–5379. <https://doi.org/10.1007/s00216-013-6972-4>
103. Franzen U, Østergaard J (2012) Physico-chemical characterization of liposomes and drug substance-liposome interactions in pharmaceuticals using capillary electrophoresis and electrokinetic chromatography. *J Chromatogr A* 1267:32–44. <https://doi.org/10.1016/j.chroma.2012.07.018>
104. Nguyen TTN, Østergaard J, Stürup S, Gammelgaard B (2013) Metallomics in drug development: characterization of a liposomal cisplatin drug formulation in human plasma by CE-ICP-MS. *Anal Bioanal Chem* 405:1845–1854. <https://doi.org/10.1007/s00216-012-6355-2>
105. Nguyen TTN, Østergaard J, Stürup S, Gammelgaard B (2013) Determination of platinum drug release and liposome stability in human plasma by CE-ICP-MS. *Int J Pharm* 449:95–102. <https://doi.org/10.1016/j.ijpharm.2013.03.055>
106. Otarola J, Lista AG, Fernández Band B, Garrido M (2015) Capillary electrophoresis to determine entrapment efficiency of a nanostructured lipid carrier loaded with piroxicam. *J Pharm Anal* 5:70–73. <https://doi.org/10.1016/j.jpha.2014.05.003>
107. Janu L, Stanisavljevic M, Krizkova S, Sobrova P, Vaculovicova M, Kizek R, Adam V (2013) Electrophoretic study of peptide-mediated quantum dot-human immunoglobulin bioconjugation. *Electrophoresis* 34:2725–2732. <https://doi.org/10.1002/elps.201300088>
108. Zhou ZM, Feng Z, Zhou J, Fang BY, Ma ZY, Liu B, Zhao YD, Hu XB (2015) Quantum dot-modified aptamer probe for chemiluminescence detection of carcino-embryonic antigen using capillary electrophoresis. *Sensors Actuators B Chem* 210:158–164. <https://doi.org/10.1016/j.snb.2014.12.087>